Investigating the effects of extrusion temperatures and material extrusion rates on FFF-printed thermoplastics

Javaid Butt (**Corresponding Author**)

javaid.butt@aru.ac.uk

Raghunath Bhaskar

raghunath.bhaskar@aru.ac.uk

Vahaj Mohaghegh

vahaj.mohaghegh@aru.ac.uk

Faculty of Science & Engineering, Anglia Ruskin University, Chelmsford, UK

Abstract

Fused filament fabrication (FFF) is one of the most widely used additive manufacturing processes in the market. It is based on material extrusion and utilises thermoplastic materials to manufacture bespoke products. The process is extremely popular due to its ease of operation and variety of available materials. To enhance the mechanical performance of parts made by FFF, reinforcements including nanoparticles, short or continuous fibers and other additives have been added to commonly used thermoplastics such as acrylonitrile butadiene styrene (ABS) and polylactic acid (PLA). Such new materials require optimization of process parameters to achieve the desired results. One such parameter is the material extrusion rate that can result in under or over extrusion leading to a variety of applications. In this study, PLA and HDPlas® PLA-GNP-A (PLA reinforced with functionalized graphene nanoplatelets) have been used to investigate the effects of material extrusion rate. An extensive comparative analysis has been provided where parts have been manufactured using a desktop 3D printer with the two materials at four extrusion temperatures (180 °C, 190 °C, 200 °C and 210 °C) and ten different extrusion rates (ranging from 70% to 160%). The study aims to evaluate the effects of extrusion temperatures and material extrusion rates on mass, dimensional accuracy, surface texture and mechanical properties of the two materials. Microstructural analysis has also been carried out to evaluate the surfaces of parts after manufacture as well as their fractured surfaces after mechanical testing to determine the impact of extrusion rate on failure modes. The results have shown that the graphene reinforced PLA material is affected more adversely by changes in material extrusion rate compared to PLA. This work provides a good comparison between two materials manufactured at four different extrusion temperatures and how the material extrusion rate can be leveraged to achieve optimal surface finish and mechanical strength.

Keywords: additive manufacturing; fused filament fabrication; PLA; graphene enhanced PLA; surface roughness; flow percentage; extrusion multiplier; material extrusion rate

1. Introduction

Additive manufacturing (AM) technologies date back to the 1980s and have become extremely prominent in the recent years due to their advantages including design freedom, cost-effectiveness, reduced waste and lead time, parts consolidation, design-driven approach leading to mass customisation and multi-scale structure design [1-7]. A wide variety of materials (e.g., metals, polymers, ceramics) in different forms (e.g., powder, sheet, filament) are available to be used with these AM technologies to manufacture highly complex and bespoke products [8, 9]. Among the different AM techniques, fused filament fabrication (FFF) is a widely used method and is based on the principle of material extrusion. It manufactures products using thermoplastics that are extruded out of a nozzle above their melting temperatures and solidify rapidly when deposited on a surface [10, 11]. Two of the most used materials for FFF are acrylonitrile butadiene styrene (ABS) and polylactic acid (PLA). They have been widely investigated and used for a variety of different applications [12, 13]. Despite

the notable advantages, parts made by FFF suffer from poor mechanical characteristics, limiting their broader adaption for end-use, fully functional and load bearing components [14, 15]. However, careful selection and subsequent optimization of different process parameters (e.g., build orientation, layer thickness, infill pattern/percentage, nozzle/bed temperature, printing speed) of the 3D printer can help to achieve the desired properties in a product. Chacón, et al., [16] studied the effects of build orientation, layer thickness and feed rate on the mechanical performance of PLA samples and provided printing guidelines to achieve desired results in terms of strength, stiffness, and ductility. Similarly, Gonabadi, et al., [17] investigated the effects of build orientation and infill pattern/density for PLA and proposed a constitutive model derived from the laminate plate theory that can help in choosing process parameters to maximise performance for a given design. Wu, et al., [18] used the orthogonal experimental design method to evaluate the influence of the layer thickness, raster angle, deformation temperature and recovery temperature on the shape-recovery ratio and maximum shape-recovery rate of PLA. They found that the shape-memory effect of PLA parts depended strongly on recovery temperature and depended more weakly on the deformation temperature and printing parameters.

Even though optimization of process parameters can help in manufacturing products with desired properties, efforts are continuously being made to enhance the properties of the commonly used thermoplastics through the incorporation of particles, fibers or nanomaterial reinforcements. Various reinforcements, such as glass fibers [19], continuous carbon fiber [20] and basalt fiber [21], have been used to enhance the mechanical properties of PLA with success. Graphene nanoplatelets (GNP) have also joined the growing list of additives to PLA. Graphene is a wonder material with a myriad of excellent properties that make it an attractive candidate for the reinforcement [22]. Caminero, et al., [23] studied the effects of GNP reinforcement on the mechanical properties, dimensional accuracy and surface texture of PLA parts and highlighted the need for optimisation of process parameters for such materials to achieve the desired mechanical behaviour of 3D printed composites.

With a variety of different process parameters, is difficult to optimise all of them and this is the reason why the default values set by software packages for different materials are used. However, no two materials are created equal. For example, PLA from one vendor might not give the same results as PLA purchased from a different vendor. The default process parameter values for a given material do not ensure the optimal result and hence require optimisation. Amid the common process parameters, one often overlooked parameter is the material extrusion rate. It is also referred to as the extrusion multiplier or flow rate or simply flow (expressed in percentage). It specifies the rate at which the printer will extrude the material. A flow rate of 100% is typically utilised to avoid issues of under extrusion (gaps/voids between layers) and over extrusion (accumulation of extra material). These common issues can lead to defective products with undesired low modulus, low toughness, and poor surface finish. Therefore, research studies are focused on identifying under/over extruded parts and limited literature is available to leverage the material extrusion rate for optimal results. For example, Tanikella, et al., [24] developed a two-step screening process (visual inspection for under extrusion followed by mass measurement) to detect under extruded parts that can help in assisting low-cost open-source 3D printers expand their range of object production to

functional parts. Jin, et al., [25] developed a real-time monitoring and autonomous correction system capable of automatically changing the printing parameters upon detecting under or over extrusion images. On the other hand, Forman, et al., [26] leveraged under extrusion to quickly print thin and flexible textiles called DefeXtiles using an unmodified 3D printer. They also explored the possibility of their approach being used for fashion design prototyping, interactive objects, aesthetic patterning, and single-print actuators. These examples show that controlling the material extrusion rate is important for different applications and can be leveraged to achieve desired results.

The literature clearly highlights the need for process parameters optimization, importance of polymer composites and limited research on leveraging extrusion temperatures and material extrusion rates for optimal results such as surface finish and mechanical strength. This study aims to investigate the effects of four different extrusion temperatures and ten extrusion rates on two materials (PLA and graphene enhanced PLA) manufactured using a desktop 3D printer. The next section (Section 2) details the materials and methods utilised in this study with particular emphasis on specimen preparation, the 3D printing process, and the testing procedures. An extensive comparative analysis is presented in Section 3 discussing the effects of extrusion temperatures and material extrusion rates on mass, dimensional accuracy, surface texture and mechanical properties of the two materials. Finally, material quality characterisation and conclusions of this work are outlined in Sections 4 and 5, respectively.

2. Materials and Methods

2.1. Materials and 3D printer

Anet® ET4 Pro (from Shenzen Anet Technology Company Limited, Hong Kong) desktop 3D printer was used to manufacture specimens according to British and International standards. The low-cost 3D printer had a build volume of 220 mm x 220 mm x 250 mm (X × Y × Z) and an extruder nozzle diameter of 0.4 mm. PrimaValue™ PLA (from Prima Creator, Sweden) [27] and HDPlas® PLA-GNP-A (from 3D Haydale Ltd., UK) [28] were used to manufacture specimens to analyze the effects of extrusion temperatures and materiel extrusion rates. From here onwards, these materials will be referred to as PLA and GPLA, respectively. PLA is a strong material that is easy to print with no unpleasant smell or hazardous fumes. It is also warp-free and provides good interlayer adhesion. On the other hand, GPLA includes HDPlas® functionalized graphene nanoplatelets of a planar size between 0.3–5 µm to improve dispersion and bonding within the PLA polymer. It provides the material with improved operating temperature performance, high rigidity, good impact strength and excellent interlayer adhesion for smooth printing.

2.2. Process Parameters and 3D Geometry

The 3D CAD models of the specimens to be built were sent to the open-source software Ultimaker Cura 4.7.1 [29] to generate G-code files and to command as well as control all the process parameters. In this study, dog-bone specimens were manufactured according to BS EN ISO 527-2:2012 [30] and the dimensions are shown in Figure 1. Four different extrusion temperatures were used to manufacture PLA and GPLA specimens with ten different extrusion rates or flow rates (expressed as a percentage in the Ultimaker Cura 4.7.1 software). Specimens

printed with 70% to 90% flow can be considered as under extruded whereas specimens printed above 100% flow can be considered as over extruded. The different process parameters used to manufacture the specimens are shown in Table 1. The appropriate process parameters were selected within Cura and the files were sliced into g-codes for printing. The two main parameters (extruder temperature and flow percentage) were modified in the 'Material' tab within the 'Print settings' of the Cura software.

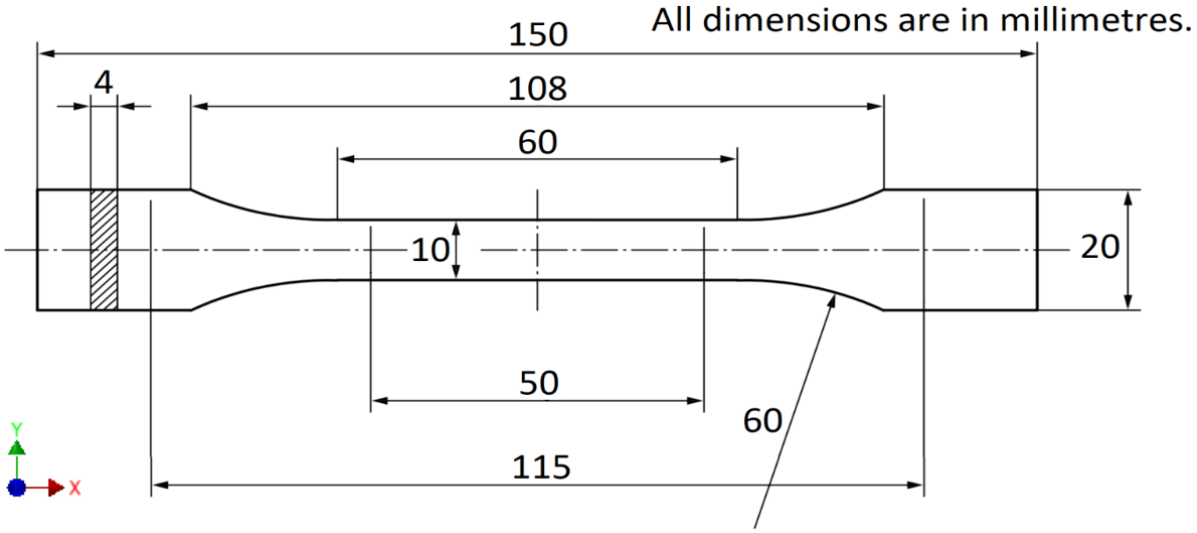

Figure 1: Dimensions of the dog-bone specimen

Table 1: Process parameters for PLA and GPLA

#	Parameters	Description
1	Infill density (%)	100
2	Infill pattern	Lines
3	Layer height (mm)	0.2
4	Nozzle size (mm)	0.4
5	Flow (%)	70, 80, 90, 100, 110, 120, 130, 140, 150, 160
6	Extrusion temperature (°C)	180, 190, 200, 210
7	Print bed temperature (°C)	60
8	Deposition speed (mm/s)	50
9	Fan speed (%)	100

2.3. Experimental Testing

Modifying the flow rate affected the dog-bone specimens in different ways as increasing or decreasing this value changed the amount of material pushed out of the nozzle over a given time interval. The mass and time required to manufacture the different specimens are shown in

Table 2 as per the Cura software. These values remained the same at different extrusion temperatures. This made measurement of mass the very first analysis point and CBK 8H weighing scale (from Adam Equipment, UK) having a resolution of 0.1g was used for this purpose. The dimensions of the dog-bone specimens were measured using a digital Vernier caliper. Due to increased material being added to the manufactured specimens, surface texture analysis was undertaken using Surftest SJ-210 (from Mitutoyo, UK) contact-type surface profilometer with a detector measuring force of 0.75 mN and a range of 360 μm [31]. Several surface parameters were quantitatively measured at micro-meter level from the specimens with the traverse direction being diagonally across the building direction at an angle of 45˚ as per ISO 4287:1997 [32]. These amplitude parameters include average surface roughness (Ra), root mean square (Rq), skewness (Rsk), and kurtosis (Rku). Other parameters such as height characterization (core roughness depth, Rk; reduced peak height, Rpk; reduced valley depth, Rvk; material portion 1, Mr1 and material portion 2, Mr2) using the linear material ratio curve ISO 13565-2:1996 standard [33] were also measured quantitatively. The parameters were selected based on recommendations from literature [34-38]. Three measurements were taken along the length of the dog-bone specimens with the measuring speed of 0.5 mm/s. The surface roughness profile was filtered through the Gaussian high-pass filter with a cut-off wavelength of 800 μm and the evaluation length being five times the sampling length.

Table 2: Mass and manufacturing times

Flow (%)	Mass (g)	Time (min)
70	7	74
80	8	74
90	9	74
100	10	74
110	11	74
120	12	74
130	13	76
140	14	76
150	15	76
160	16	76

After surface analysis, the dog-bone specimens were subjected to ultrasonic testing using a Proceq PUNDIT® PL-200 (from Test Equipment Center, Japan) comprising two 54 kHz transducers [39]. This non-destructive test utilises high-frequency sound waves to detect flaws and defects in products as well as take measurements e.g., thickness. The dog-bone specimens were tested at three points along their length to ascertain an average value of transmission time (μs). For tensile testing, three specimens of each configuration were manufactured and tested as per BS EN ISO 527-2:2012. The testing was carried out using a Tinius Olsen Universal Tensile Testing Machine at a crosshead speed of 1.5mm/s according to the standard. Microstructural analysis was undertaken using a JCM-5000 NeoScope™ tabletop scanning electron microscope (SEM) before and after the tensile testing. It was done before to visualise the gaps or the accumulation of material at different flow percentage levels on the surface. After the tensile test, this helped to investigate the fracture mechanism. The fractured surfaces

were carefully cut to size to fit atop the platform of the SEM. No surface treatment was applied to avoid contamination of the fractured surfaces.

3. Experimental Results and Discussions

3.1. Measurement of Mass

The flow percentage is set at 100% by default in the Cura software and based on this value, Cura automatically calculates how fast to move the extruder motor for certain print speeds or filament diameters. The primary reason for modifying this parameter is to avoid over or under extrusion as all 3D printing filaments do not behave the same at different extrusion temperatures [24, 26]. Most materials can be extruded at a flow rate between 90% and 110% to get good surface finish and appropriate strength. With a lower flow rate, the amount of material in a given cross-sectional area would be less compared to a higher flow rate with the same 3D CAD model. Furthermore, a thicker product would exhibit a higher fracture load compared to a thinner material provided appropriate interlayer adhesion. As the flow rates were modified for the dog-bone specimens, their mass was measured using the CBK 8H weighing scale. These mass values were compared to the values provided by the Cura software in Table 2 and the percentage differences are plotted in Figure 2 for PLA and GPLA.

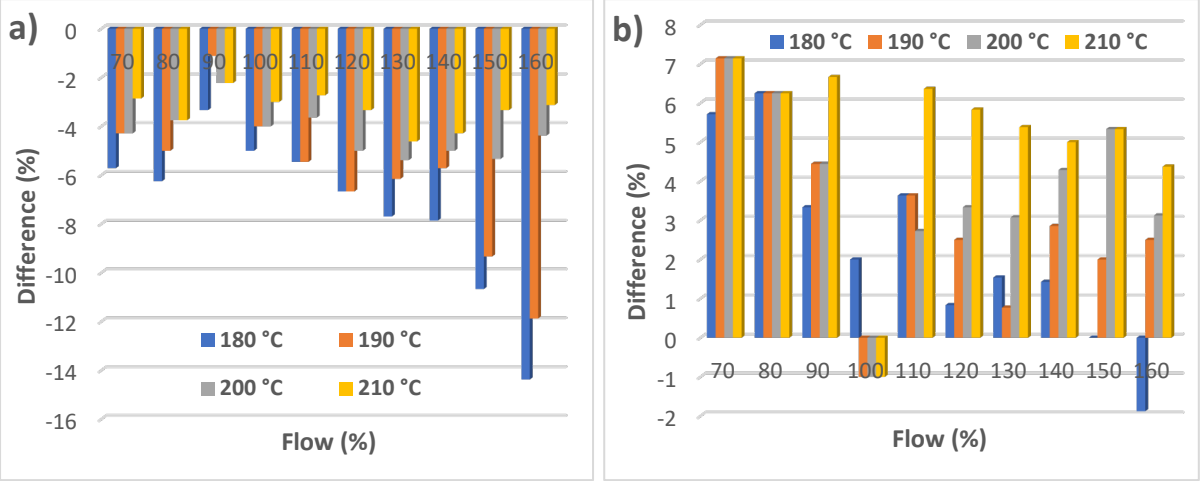

Figure 2: Percentage differences: a) PLA mass measurements; b) GPLA mass measurements

It is clear from Fig. 2a that the mass of PLA specimens did not increase for any of the temperatures or flow percentages. Furthermore, specimens manufactured at 180 °C exhibited the highest negative percentage change of all the extrusion temperatures starting at 5.7% for 70% flow and moving to 14.37% at 160% flow. Extrusion temperature of 190 °C also exhibited high negative percentage change values whereas 200 °C and 210 °C showed relatively smaller variations especially at high flow percentages (150% and 160%). The extrusion temperature of 210 °C also exhibited the lowest negative percentage change with 2.86% at 70% flow and only 3.12% at 160% flow. These measurements indicate that PLA did not accumulate excess material and showed lower mass values compared to the ones indicated by the Cura software.

On the other hand, Fig. 2b showed a different scenario where almost all the specimens exhibited positive percentage changes as high as 7.14%. Extrusion temperature of 180 °C showed positive change at all flow percentages except for 160% where the negative percentage change was recorded as 1.87%. At the same time, all the other extrusion temperatures showed negative percentage change of exactly 1% at 100% flow indicating that GPLA material require

optimisation of the flow percentage value to avoid over or under extrusion. An increased positive percentage change can also be observed in Fig. 2b with increasing extrusion temperatures. At 160% flow, the values indicate positive percentage change of 2.5%, 3.12% and 4.37% for extrusion temperatures of 190 °C, 200 °C and 210 °C, respectively.

3.2. Dimensional Analysis

All the specimens were measured for deviations from their original dimensions using a digital Vernier caliper. As more material is added to the specimens at high flow percentages, over extrusion becomes a serios problem as can be seen from Figure 3. The opposite applies with lower flow percentages leading to under extrusion characterised by larger voids or gaps between layers. Over/under extruded parts can look significantly different from a standard 100% flow percentage part and can also behave differently under loading conditions. In addition to having effects on strength properties, flow also affects the dimensional accuracy of these parts making them harder to place in assemblies where a tight fit is required.

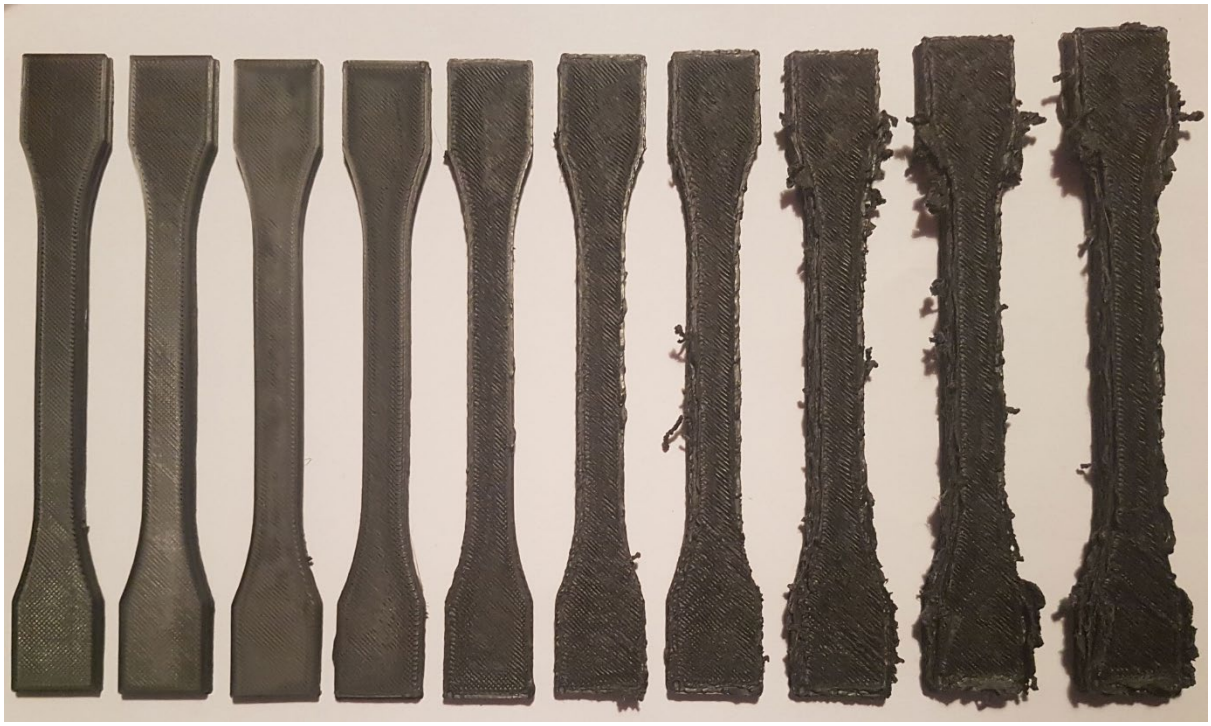

Figure 3: GPLA specimens printed at extrusion temperature of 200 °C (left to right showing 70% to 160% flow percentages)

The excess material clearly visible in Fig. 3 adds to the mass of the specimens as discussed in Section 3.1 and also affects their geometrical accuracy. The percentage differences in all the three axes (X, Y and Z) for PLA and GPLA are shown in Fig. 4. Due to a lower flow percentage leading to a lack of material, both PLA and GPLA showed negative percentage changes along the X-axis from 70% to 90% flow before switching to positive percentage changes from 100% flow onwards as can be observed in Figs. 4a and 4b. Along the X-axis for PLA, the extrusion temperature of 180 °C exhibited the lowest percentage change at 0.134% for 160% flow whereas the highest was observed for 210 °C at 1.34% for 160% flow (Fig. 4a). On the other hand, GPLA showed comparatively larger differences along the X-axis. Fig. 4b shows an increase in percentage change with increased extrusion temperatures. At 180 °C and 190 °C, the positive percentage change was 1%, increasing to 1.67% (200 °C) and then 1.73%

(210 °C) for 160% flow as seen in Fig. 4b. These results indicate that increased extrusion temperatures and flow percentages affected GPLA more than PLA along the X-axis.

The dimensional changes along the Y-axis for PLA are shown in Fig. 4c with negative percentage changes only observed at 70% and 80% flow for all extrusion temperatures before moving to positive percentage change for all the other flow rates. As seen in Fig. 4a, the extrusion temperature of 180 °C exhibited the lowest percentage change at 3.5% for 160% flow. At flow percentage of 160%, the highest change was observed at 5% for 190 °C, 4.5% for 210 °C, 4% for 200 °C and finally 3.5% for 180 °C. Fig. 4d shows GPLA with negative percentage change at 70% flow for all the extrusion temperatures before moving to positive percentage changes. Similar to Fig. 4b, GPLA exhibited significant changes along the Y-axis with the highest value being 14% at 210 °C for 160% flow. This was followed by 13% at 200 °C, 12.5% at 190 °C and 11% at 180 °C. This show that as the extrusion temperature increased, more material was accumulated along the Y-axis leading to significant deformation in GPLA.

Thickness is an important geometrical aspect and could lead to significant issues both in terms of part aesthetics and mechanical performance. Under extrusion at 70%, 80% or 90% should lead to lower thickness whereas over extrusion from 100% above should lead to a higher thickness value of the dog-bone specimens. Fig. 4e showed the variations in thickness or along the Z-axis for PLA with significantly smaller thickness values until 100% flow. It clearly indicates the usefulness of optimising the flow percentage for a given material to ensure dimensional accuracy and consistency. The thickness increased significantly from 110% flow onward as well as the positive percentage change with increasing extrusion temperatures. The lowest value at 160% flow was observed at 17.5% for 180 °C, 30% for 190 °C, 32.5% for 200°C and finally 35% for 210 °C. GPLA followed a similar pattern in Fig. 4f as PLA, but only exhibited smaller thickness values until 90% flow as opposed to 100% flow for PLA. The results along the Z-axis were consistent for all the extrusion temperatures at 100% flow. With increase in flow, the thickness also increased drastically for all the extrusion temperatures. Thickness as high as 6mm was observed (as opposed to 4mm) at 160% flow for 210 °C indicating a positive percentage change of 50%. The smallest value at 160% flow was observed for 190 °C at 45%. Upon comparison of the thickness change, it is clear that the thickness of GPLA specimens (6mm at 210 °C) at 160% flow increased more compared to PLA (5.4mm at 210 °C) in addition to the overall high positive percentage change values. Overall, it is evident from Fig. 4 that the dimensional accuracy of GPLA was more adversely affected by the increased extrusion temperatures and flow percentages along the three axes compared to PLA.

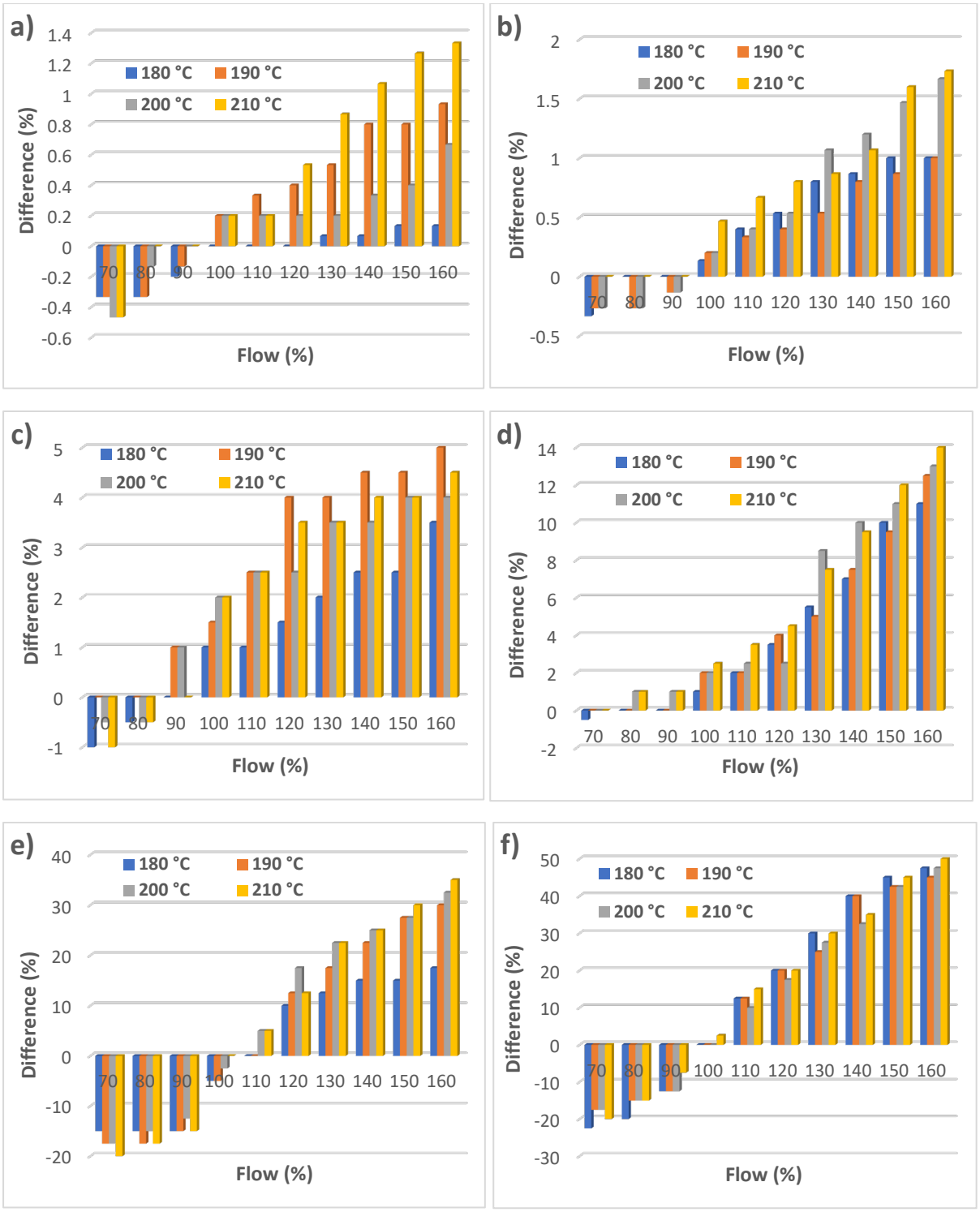

Figure 4: Dimensional analysis: a) Percentage change along X-axis for PLA; b) Percentage change along X-axis for GPLA; c) Percentage change along Y-axis for PLA; d) Percentage change along Y-axis for GPLA; e) Percentage change along Z-axis for PLA; f) Percentage change along Z-axis for GPLA

3.3. Surface Roughness Analysis

Over and under extrusion are issues faced by FFF systems [24, 25] and commonly used options for mitigation are the optimisation of the extrusion temperature and/or flow percentage. Over extrusion means accumulation of excess material and can lead to dimensional inaccuracy, layer drooping, stringing, oozing and blobs. On the other hand, under extrusion is characterised

by large voids/gaps between layers and can also be caused by low print temperatures, high print speeds and clogged nozzles. It can also lead to poor bridging performance, layer delamination and poor bed adhesion. These issues can be resolved by dispensing slightly more material or over extruding. However, flow percentage is only one parameter and achieving excellent surface finish requires optimisation of several factors. In this study, extrusion temperatures and flow percentages were changed whereas all the other parameters remained constant. This led to most over extruded specimen for both PLA and GPLA showing extremely poor surface finish as demonstrated in Fig. 3 (Section 3.2) with peak/valley measurements exceeding the 360 µm range of the Surftest SJ-210 contact-type surface profilometer. Only PLA printed at 200 °C was properly measured for all the different flow percentages whereas GPLA specimens could only be measured up to 120% due to the extremely poor surface finish. This was expected as the dimensional accuracy of GPLA was affected more adversely compared to PLA (Section 3.2). Therefore, the specimens shown in this section range from 70% to 120% flow for both PLA and GPLA measured with the traverse direction being diagonally across the building direction at an angle of 45˚. The average surface roughness (Ra) measured along the length of the dog-bone specimens is shown in Fig. 5 and highlights two clear patterns for both PLA and GPLA. Firstly, the surface roughness is higher for the under extruded specimens before becoming the lowest and then moving to high values again for the over extruded specimens at all extrusions temperatures. Secondly, the highest extrusion temperature (210 °C) shows the highest surface roughness value at 120% flow.

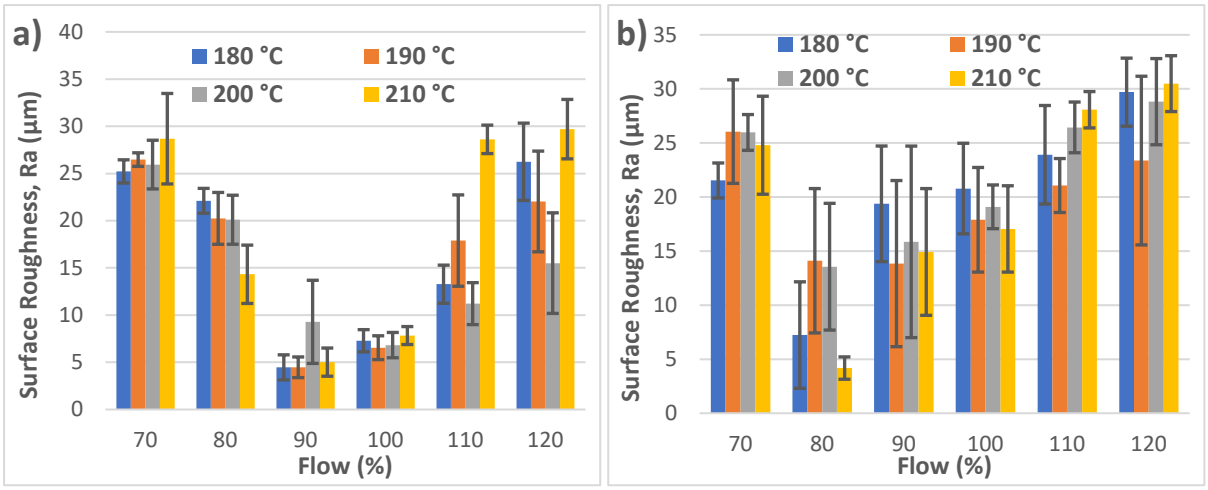

Figure 5: Surface roughness measurements: a) PLA material; b) GPLA material

It is evident from Fig. 5a that the lowest surface roughness value was observed at 90% flow for 180 °C, 190 °C and 210 °C extruding temperatures whereas 200 °C demonstrated the lowest value at 100% flow for PLA. This indicate that optimal surface finish can be achieved at 90% flow at the three aforementioned temperatures. It is also interesting to note that 70% and 80% flow specimens (under extruded) showed values as high as over extruded specimens at 110 % and 120% flow indicating the gaps (peak/valley measurements) formed by under extrusion can match the over extruded specimens to a certain extent. GPLA also show a similar picture as PLA in Fig. 5b with the lowest values being observed at 80% flow and then gradually moving upward until 120% flow for all the extrusion temperatures. The only exception was 190 °C that showed a slightly lower surface roughness at 13.8 µm for 90% flow as opposed to

14.1 µm for 80% flow. Overall, the surface roughness of both PLA and GPLA remained quite close and did not show drastic differences in the minimum or maximum values. These results indicate that different flow percentages satisfy the aesthetics or surface finish requirements for various materials and should be kept in mind while manufacturing products using FFF.

The two-dimensional (2D) surface profile ratios of Rq/Ra for PLA and GPLA are shown in Fig. 6. For PLA in Fig. 6a, the ratio of the average root means square (Rq) to average surface roughness (Ra) was found to be randomly varying with deviation of around 1.26 ± 0.078 for 180 °C, 1.28 ± 0.069 for 190 °C, 1.29 ± 0.107 for 200 °C and 1.29 ± 0.104 for 210 °C. These deviations are very small and are tolerable for all the flow percentages at the different extrusion temperatures. Fig. 6b showing the Rq/Ra for GPLA was randomly varying with deviation of around 1.27 ± 0.044 for 180 °C, 1.28 ± 0.053 for 190 °C, 1.28 ± 0.060 for 200 °C and 1.26 ± 0.069 for 210 °C. Both PLA and GPLA showed similar mean values for Rq/Ra whereas the standard deviation values for GPLA increased with increase in extrusion temperature. Ideally, Rq/Ra equal to 1.22 (for 2D) with minimum deviation is an excellent surface profile ratio, as the Rq is very sensitive to peaks and valleys than Ra because the amplitudes are squared [40].

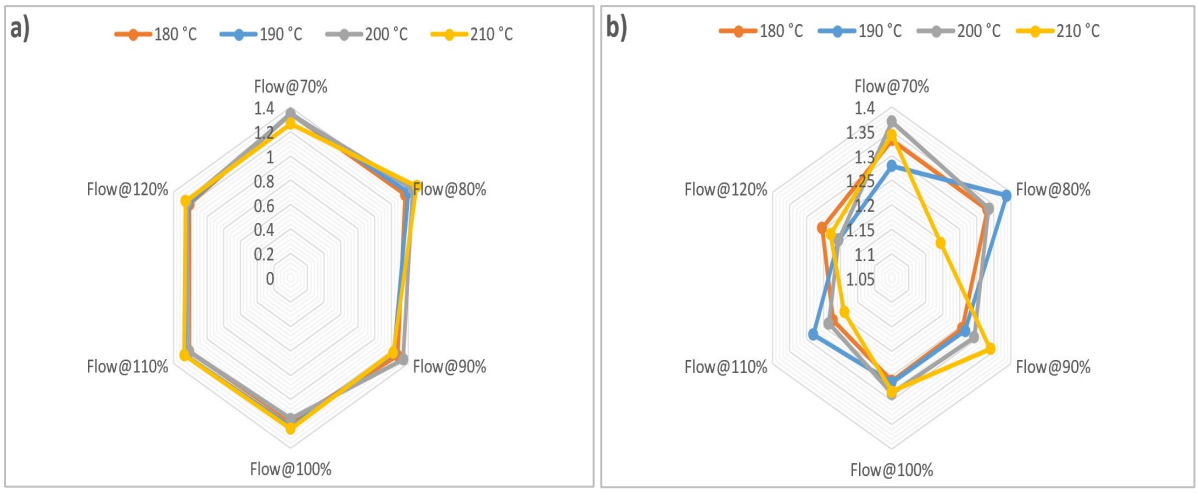

Figure 6: Two-dimensional surface profile ratio: a) PLA material; b) GPLA material

3.3.1. Skewness and Kurtosis

The third central moment skewness (Rsk) and the fourth central moment kurtosis (Rku) for PLA and GPLA are shown in Fig. 7. Ideally, a value of zero for skewness and three for kurtosis is typical for a random, Gaussian profile and weakly isotropic [40, 41]. In Fig. 7a, the trend of PLA showed an overall negative skew (negative for flat peaks and steep valleys representing a surface with a top plateau with deep grooves or pores) at 70% and 80% flow for all the extrusion temperatures. All the specimens printed at 90% flow or above showed an approximately symmetrical skew (except for 100% flow at 210 °C that showed a high positive skew). The maximum and minimum trend of skewness was in the range of $-1.297 \leq Rsk \leq -0.616$ for 180 °C, $-0.969 \leq Rsk \leq 0.411$ for 190 °C, $-0.149 \leq Rsk \leq 0.202$ for 200 °C and $-1.06 \leq Rsk \leq 0.694$ for 210 °C. In Fig. 7b, the trend of GPLA also showed an overall high negative skew at 70% and 80% flow for all the extrusion temperatures (except for 80% flow at 210 °C that shows an approximately symmetrical skew). All the 90% flow specimens exhibited a high positive skew (positive for steep peaks and flat valleys representing a surface with a flat

bulk and high peaks as if particles were deposited on a plane) along with 100% flow at 210 °C and 110% flow for 190 °C specimens. The remaining specimens exhibited an approximately symmetrical skew. The maximum and minimum trend of skewness was in the range of −0.981 ≤ Rsk ≤ 0.497 for 180 °C, −1.467 ≤ Rsk ≤ 1.056 for 190 °C, −1.24 ≤ Rsk ≤ 1.15 for 200 °C and −1.303 ≤ Rsk ≤ 1.246 for 210 °C.

In Fig. 7c, the maximum and minimum trend of kurtosis for PLA was in the range of 3.045 ≤ Rku ≤ 4.262 for 180 °C, 2.518 ≤ Rku ≤ 4.704 for 190 °C, 1.954 ≤ Rku ≤ 3.837 for 200 °C and 2.655 ≤ Rku ≤ 5.680 for 210 °C. Based on the kurtosis results, 190 °C, 200 °C and 210 °C showed leptokurtic (longer and fatter tails with a high and sharp central peak) and platykurtic (narrow distribution with a few extreme points above and below while most points are concentrated around the mean value) distribution with high and low degree of peakedness as Rku represent values both less and greater than 3. The only temperature to show a mesokurtic (normal) distribution in addition to leptokurtic and platykurtic was 180 °C. In Fig. 7d, the maximum and minimum trend of kurtosis for GPLA was in the range of 2.517 ≤ Rku ≤ 4.090 for 180 °C, 2.338 ≤ Rku ≤ 5.105 for 190 °C, 2.118 ≤ Rku ≤ 4.627 for 200 °C and 2.255 ≤ Rku ≤ 4.741 for 210 °C. Based on the kurtosis results, all the extrusion temperatures showed leptokurtic and platykurtic distribution for GPLA. PLA and GPLA exhibited different results for skewness and kurtosis values. Majority of the PLA specimens showed an approximately symmetrical skew with under extruded specimens (70% and 80% flow) showing negative skew. On the other hand, GPLA showed a mixture of negative, approximately symmetrical, and positive skew specimens highlighting more material deposition due to over extrusion. For PLA, kurtosis showed a clear trend with values higher than 3 for under extruded specimens (70% and 80% flow) and lower for all the others (except for 100% and 110% flow at 210 °C). GPLA showed a mixture of values higher and lower than 3 for kurtosis and highlight that the effect of flow percentages at different extrusion temperatures result in more variations than PLA.

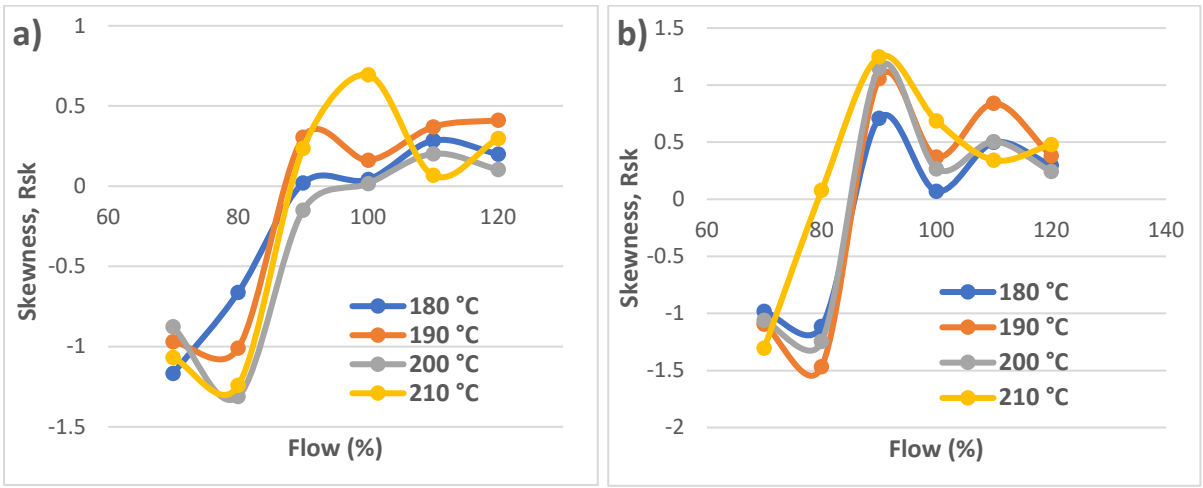

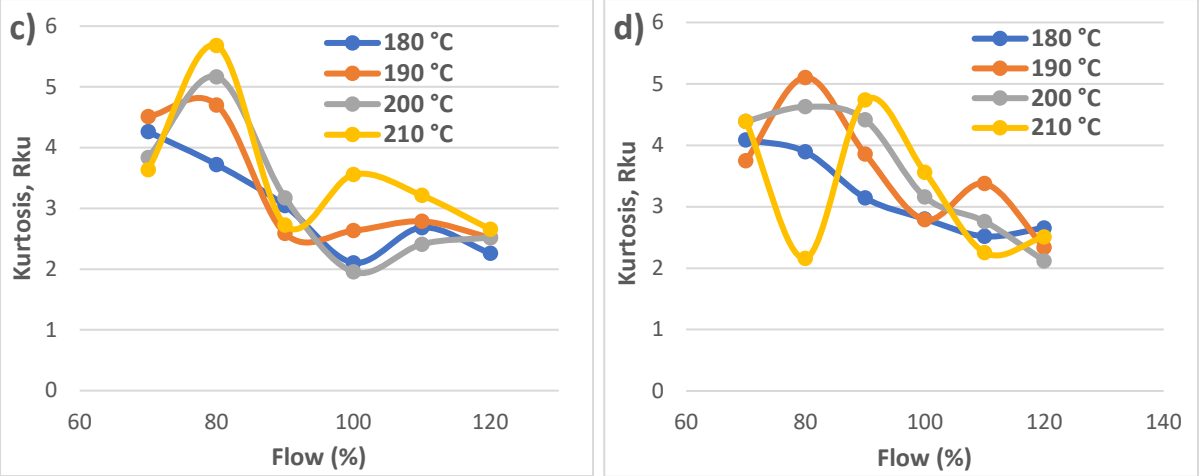

Figure 7: Skewness and kurtosis: a) PLA skewness curves; b) GPLA skewness curves; c) PLA kurtosis curves; d) GPLA kurtosis curves

3.3.2. Height Characterization

The Rk group parameter (Rk, Rpk, Rvk, Mr1, and Mr2) is derived from the bearing ratio curve based on the ISO 13565-2:1996 standard (Abbott curve, which represents the cumulative probability density function of the profile height of a surface and can be calculated by integrating the profile trace). Rk (µm) represents the core/kernel of the printed specimens, Rpk (µm) and Mr1 (%) represent the peaks of the specimens whereas Rvk (µm) and Mr2 (%) represent the valleys of the 3D printed specimens. These parameters were precisely designed for the control of the potential wear in cylinder bores in the automotive industry. They numerically describe the wear characteristics of the bore by use of a material ratio curve [40]. In this study, Rk (core), Rpk (peaks) and Rvk (valleys) were examined for both PLA and GPLA. The bearing area provides information about the extent of the surface behaviour above a certain height. The Rpk and Rvk parameters can influence the friction characteristics. Large Rk parameter implies a surface composed of high peaks providing small initial contact area and thus high contact stress areas when the surface is contacted [40]. This is to be expected in this work as high flow percentages have been used to manufacture specimens.

The mean and SD values of Rk, Rpk and Rvk for PLA at different extrusion temperatures are shown in Fig. 8. It is evident that 90% and 100% flow specimens exhibit the lowest values indicating a good surface finish at all the four extrusion temperatures. Furthermore, under extrusion specimens exhibit low core and peak values but high valley measurements due to the lack of material. These values move upward for the over extruded specimens due to the presence of excess material. The optimal results were observed for 200 °C (Fig. 8c) with all the three parameters (except for higher valley measurements for under extruded specimens) showing relatively lower values compared to other temperatures in Figs. 8a, 8b and 8d.

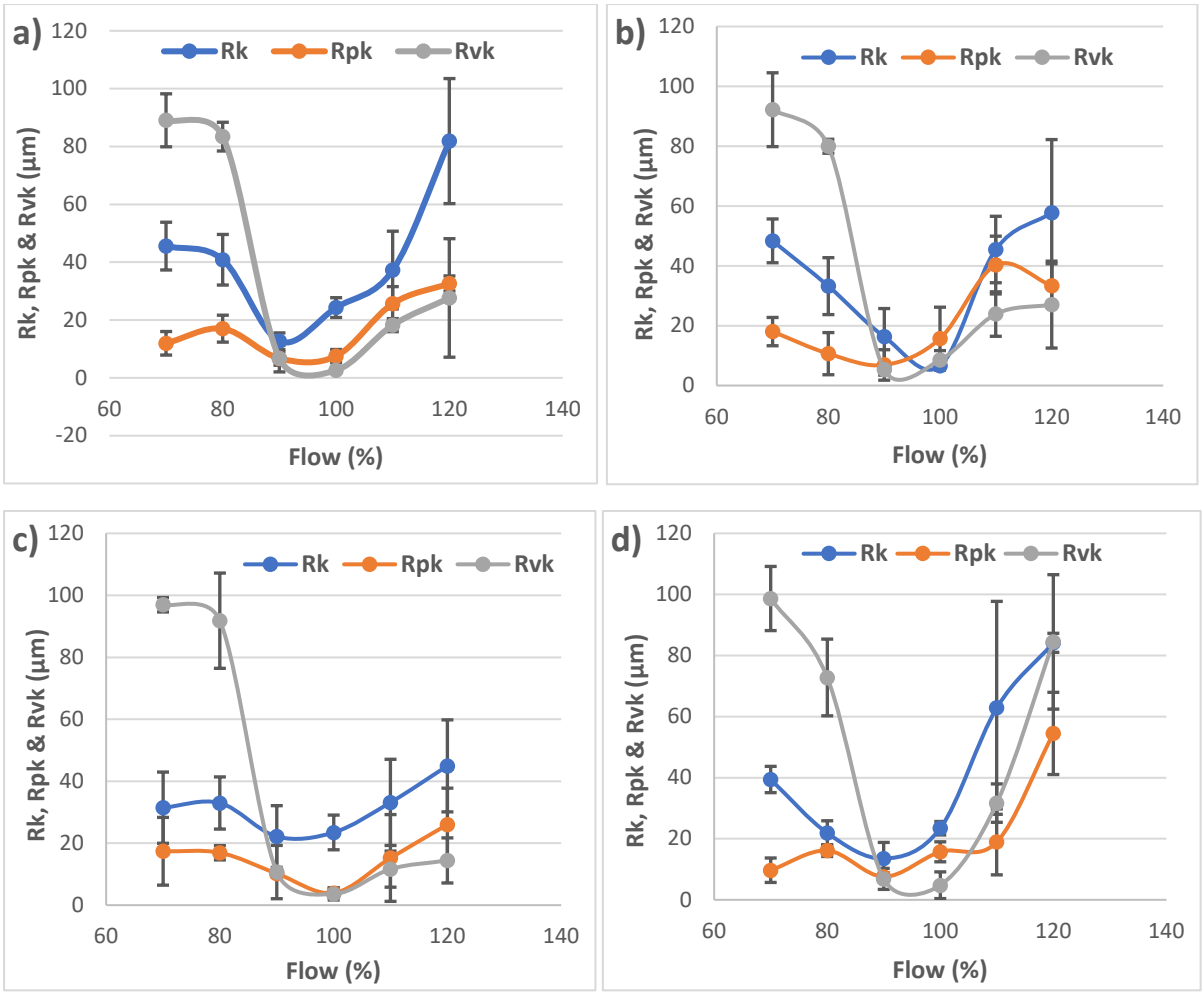

Figure 8: Rk, Rpk and Rvk assessment at different temperatures for PLA: a) 180 °C; b) 190 °C; c) 200 °C; d) 210 °C

The mean and SD values of Rk, Rpk and Rvk for GPLA at different extrusion temperatures are shown in Fig. 9. As opposed to PLA, 80% and 90% flow exhibit the lowest values in this case (except for 90% flow at 180 °C in Fig. 9a) for all the extrusion temperatures. Except for these two flow percentages, the values are high for all other specimens whether under or over extruded. Temperatures of 180 °C in Fig. 9a and 210 °C in Fig. 9d also exhibit the highest values compared to 190 °C and 200 °C in Figs. 9b and 9c, respectively. These results indicate that GPLA is affected more adversely than PLA based on the changes in extrusion temperatures and flow percentages.

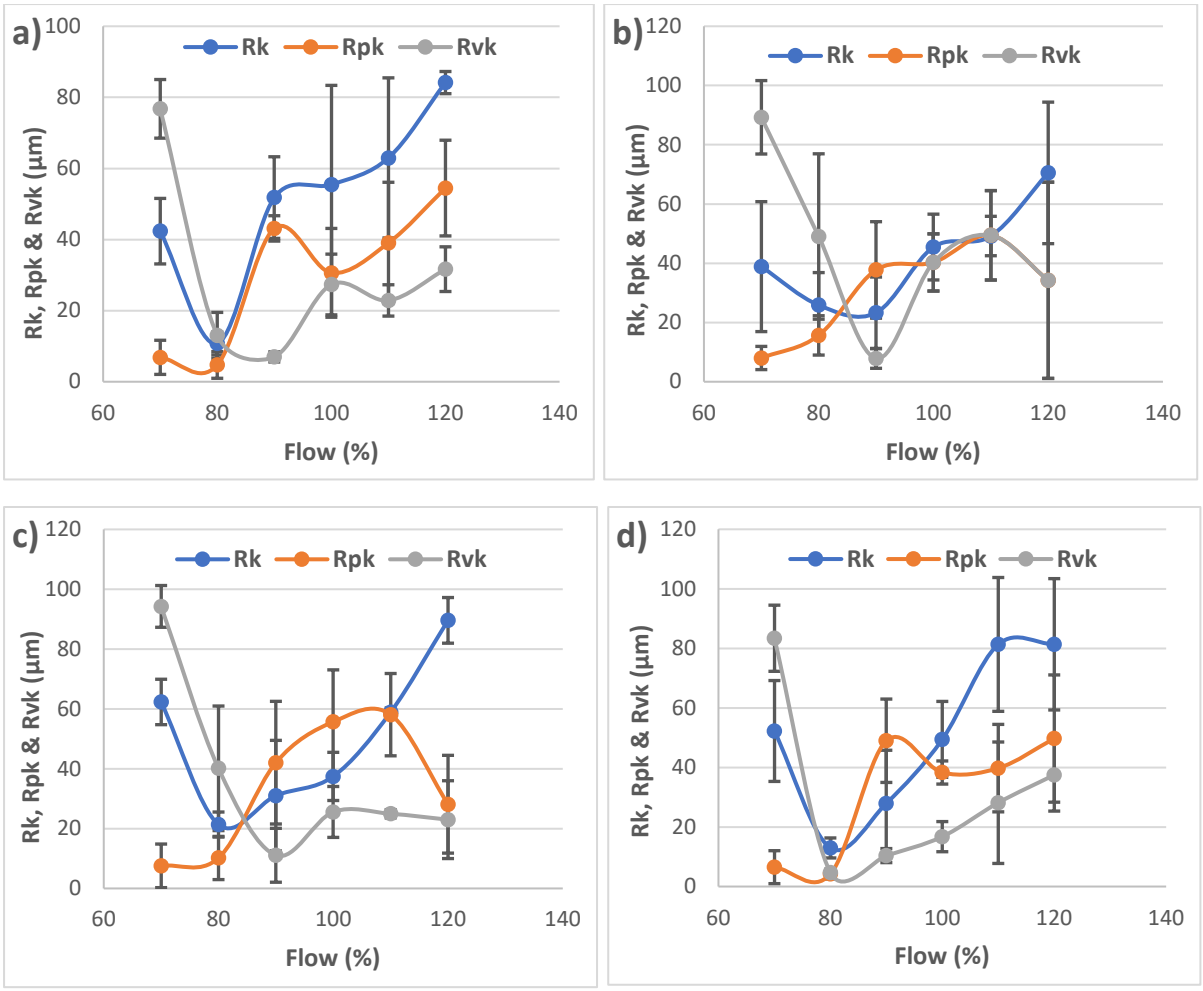

Figure 9: Rk, Rpk and Rvk assessment at different temperatures for GPLA: a) 180 °C; b) 190 °C; c) 200 °C; d) 210 °C

Figure 10 shows the material ratio assessment (Mr1 & Mr2) for PLA at different extrusion temperatures. It corresponds to the upper and lower limit position of the roughness core. It is evident that Mr1 shows comparatively smaller material portion with less than 20% for all extrusion temperatures whereas Mr2 shows large material portion by more than 80% (except at 70 % flow for all temperatures). These results indicate that PLA exhibit approximately ~20% flat peaks over roughly ~80% steep valleys, which is consistent with the results obtained from skewness and kurtosis (Fig. 7). On the other hand, the material ratio assessment for GPLA shown in Fig. 11 is not as consistent as PLA. Mr1 is less than 20% for 180 °C and 210 °C whereas it is slightly over for 190 °C and 200 °C. Similar trend was observed for GPLA when Rk, Rpk and Rvk were measured (Fig. 9). Consequently, Mr2 is above 80% for 180 °C and 210 °C (except for 80% flow at 180 °C) whereas it is lower for 70% and 80% flow at 190 °C as well as 80% flow at 200 °C.

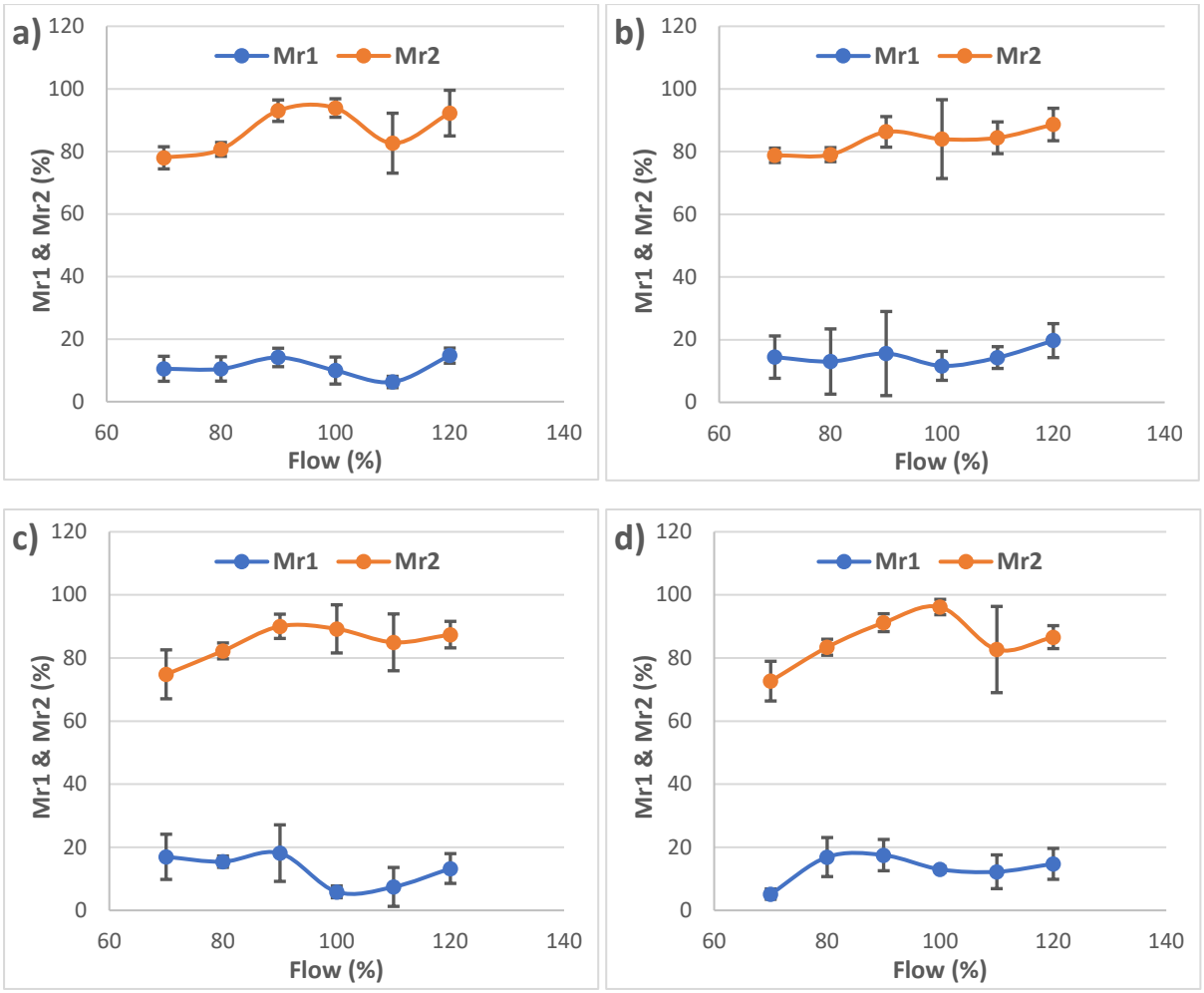

Figure 10: Material ratio assessment at different temperatures for PLA: a) 180 °C; b) 190 °C; c) 200 °C; d) 210 °C

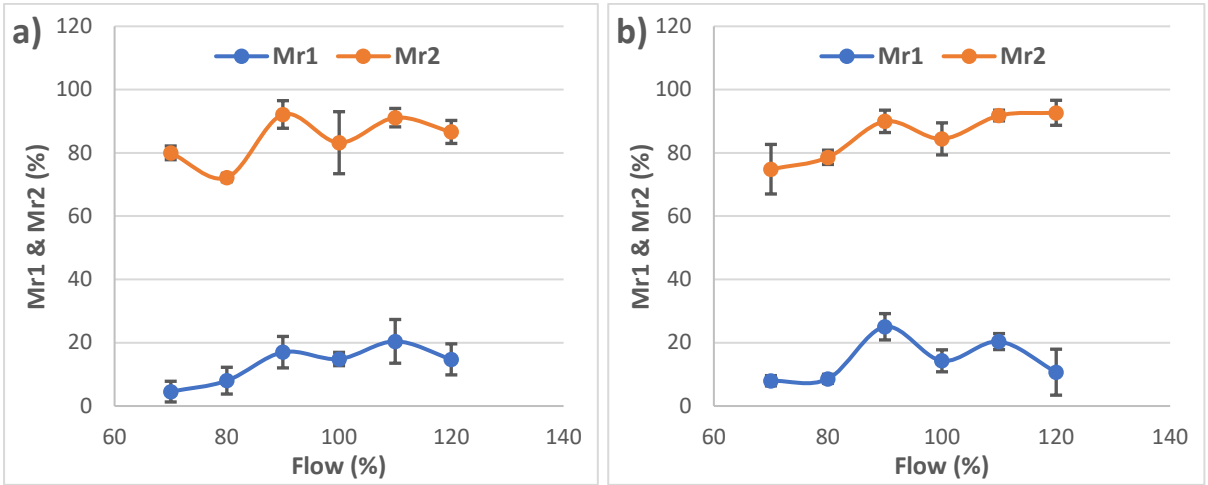

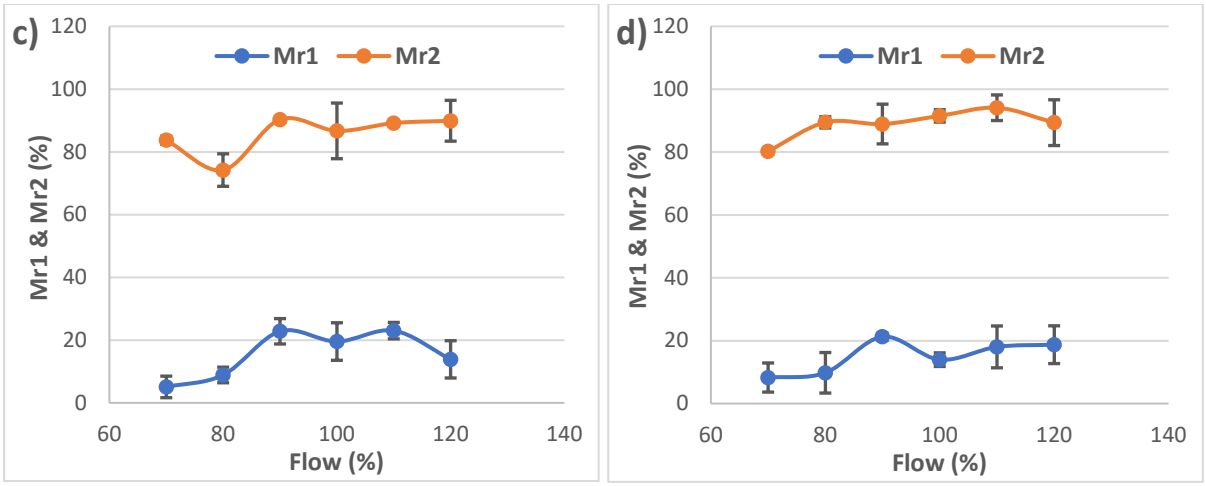

Figure 11: Material ratio assessment at different temperatures for GPLA: a) 180 °C; b) 190 °C; c) 200 °C; d) 210 °C

3.4. Ultrasonic Testing

This nondestructive test can help to detect defects in the manufactured specimens [19, 42]. In under extruded specimens, gaps are present between the individual layers due to less material whereas the layers are more closely packed for over extruded specimens. However, specimens manufactured at high flow percentages show extremely poor surface finish making inspection difficult. Ultrasonic test was conducted on all the dog-bone specimens and three measurements were taken along their length. The time taken by the high frequency acoustic sound waves to travel from one transducer through the dog-bone specimen and to the second transducer is measured and the results are shown in Figure 12.

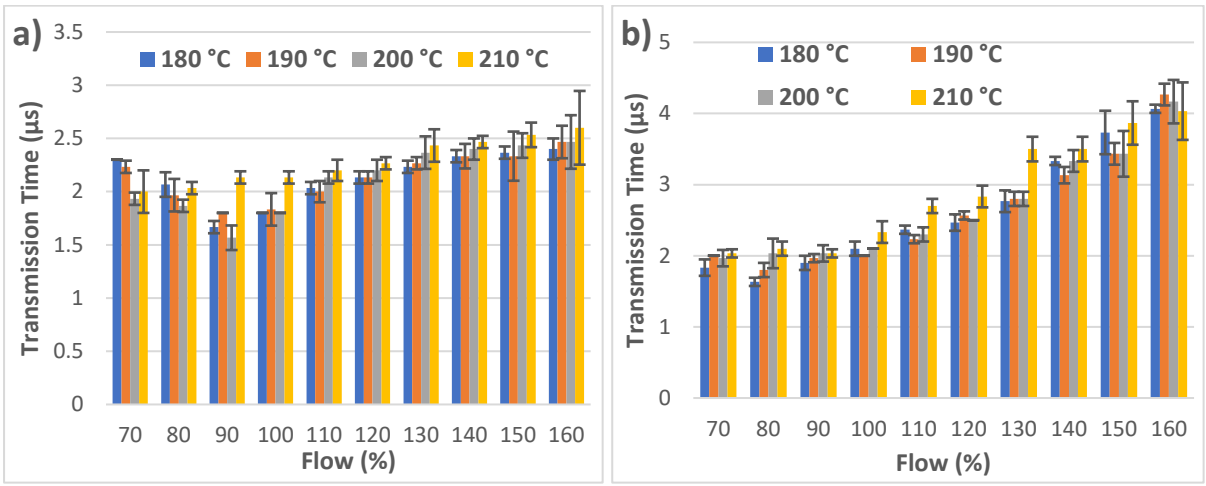

Figure 12: Results from ultrasonic testing: a) PLA material; b) GPLA material

In Fig. 12a, PLA showed higher values for the under extruded specimens until reaching the lowest transmission times at 90% flow. The values increased gradually from 90% flow as the thickness of the specimens also increased. The maximum thickness reached for PLA specimens was 5.4 mm (Section 3.2) at 160% flow for 210 °C and it showed a transmission time of 2.6 µs. The lowest thickness (3.2 mm) was also for 210 °C at 70% flow and the time recorded was 2 µs. This showed that with a difference of 2.2 mm, the transmission time went up only 0.6 µs. On the other hand, GPLA transmission times in Fig. 12b showed a gradual

increase from 70% to 160% flow. The under extruded specimens did not suffer as much as with PLA. However, the over extruded specimens showed very high values compared to PLA. The lowest values for GPLA were obtained for 90% flow (similar to PLA) and increased as high as 4.2 µs at 160% flow for 190 °C. The maximum thickness reached for GPLA specimens was 6 mm (Section 3.2) at 160% flow for 210 °C and it showed a transmission time of 4.03 µs. The lowest thickness (3.1 mm) was for 180 °C at 70% flow and the time recorded was 1.8 µs. The difference between the transmission time of the thickest and the thinnest specimen is 2.23 µs. This highlight that more time is required by the sound waves to travel through GPLA specimens indicating either defects or large voids that offer resistance. These results also indicate that GPLA is affected more adversely with the increase in flow percentages compared to PLA at the same extrusion temperatures.

3.5. Tensile Testing

Force vs displacement curves for PLA and GPLA are shown in Fig. 13. Decreasing or increasing the flow percentage result in under or over extruded specimens, respectively. Under extruded specimens are thinner with gaps/voids between layers whereas over extruded specimens result in tightly packed rows of extruded material leading to minimal voids and gaps between layers. The minimal voids result in a much larger bonding surface between printed rows and improved strength properties as well as higher thickness compared to the 3D CAD model (4 mm). In Fig. 13a, the 70% and 80% flow PLA specimens fractured at very low values with the highest being observed at 1065N for 210 °C (80% flow) specimen and the lowest was 610N for 180 °C at 70% flow. The 90% flow specimens showed a substantial increase over the 70% and 80% specimens with the fracture load values rising with increased flow percentages. Specimens printed at 180 °C showed a consistent rise in fractur load values (1688N) that continue to increase until 150% flow where the highest value was observed at 2313N and then a sharp decline at 160% flow with 2107N. This pattern was consistent with all the other extrusion temperatures as well where the fracture load values kept increasing until 150% flow and then showed a sharp decline for 160% flow specimens. It is important to note that the thickness of the specimens kept increasing and consequently the fracture load should increase as well. However, there had to be a limit to how much material can be added to a specimen before the additional material stopped being useful. This was the case with the 160% specimens with extremely rough surface finish that led to stress risers on the surface causing premature failure of the specimens. Another important consideration would be the use of flow percentages to manufacture stronger parts in a timely manner with good surface finish. Based on the results obtained in this work for PLA, it is clear that 120% flow specimens (Section 3.3) can provide good surface finish and high tensile strength for all extrusion temperatures. For applications where surface finish is not a consideration and high mechanical strength is needed, enhancing the flow percentage to as high as 150% can result in the ideal product.

In Fig. 13b, GPLA showed a gradual increase in fracture load values as well. It was more consistent compared to PLA where there was a significant difference between 70% or 80% flow specimens and 90% flow specimens. Unlike having the same flow percentage showing the highest fracture load values for all temperatures, GPLA showed varying results. At 180 °C, the fracture load values kept rising until 150% flow (2089N) and decreased slightly

at 160% flow (2070N). At 190 °C, the fracture load values kept rising and did not decrease showing that more material could potentially be added at 170% to manufacture a stronger product. At 200 °C, the fracture load values showed a downward trend similar to PLA with the highest value at 150% flow (2272N) and then a decline at 160% flow (2123N). Extrusion temperature of 210 °C was different as it showed the highest fracture load value at 140% flow (2143N) and then a decrease at the subsequent flow percentages. Overall, PLA showed more consistent results compared to GPLA with the latter showing the capacity to increase the flow percentage beyond 160% at 190 °C as opposed to the former that can only sustain until 150% flow.

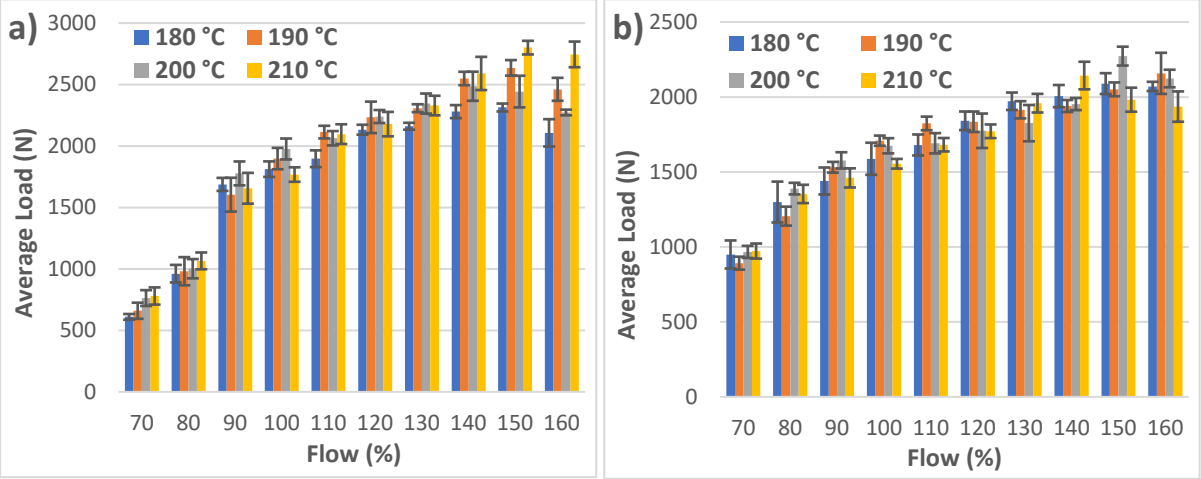

Figure 13: Results from tensile testing with standard deviation as error bars: a) PLA material; b) GPLA material

3.6. Microstructural Analysis

To highlight the significance of under and over extrusion, SEM micrographs were first taken of the surfaces of PLA and GPLA specimens printed at 200 °C as a reference. Figure 14 shows the micrographs for PLA and clearly highlights the under and over extrusion of the material. The 70% flow specimen in Fig. 14a shows clear gaps between layers whereas 100% flow specimen (Fig. 14b) shows an almost perfect alignment with little to no gaps between layers. This is also supported by the surface roughness results discussed in Section 3.3 (Fig. 5) where the PLA specimen printed with 100% flow at 200 °C showed the lowest surface roughness at 6.82 µm. The over extruded specimens in Figs. 14c and 14d at 130% and 160% flow show tightly packed rows of extruded material but with slight peaks as the excess material accumulated within the printed specimens. It is to be noted that PLA printed at 200 °C showed peaks/valleys within the 360 µm limit of the profilometer; hence, the reason for a good surface finish even at 160% flow (Fig. 14d). On the other hand, GPLA printed at 200 °C show slightly different results for the over extruded specimens in Figure 15. The specimens printed with 70% flow (Fig. 15a) and 100% flow (Fig. 15b) show similar characteristics as the ones printed from PLA. However, the over extruded specimens at 130% flow (Fig. 15c) and 160% flow (Fig. 15d) show high peaks and deep valleys resulting in extremely rough surface finish.

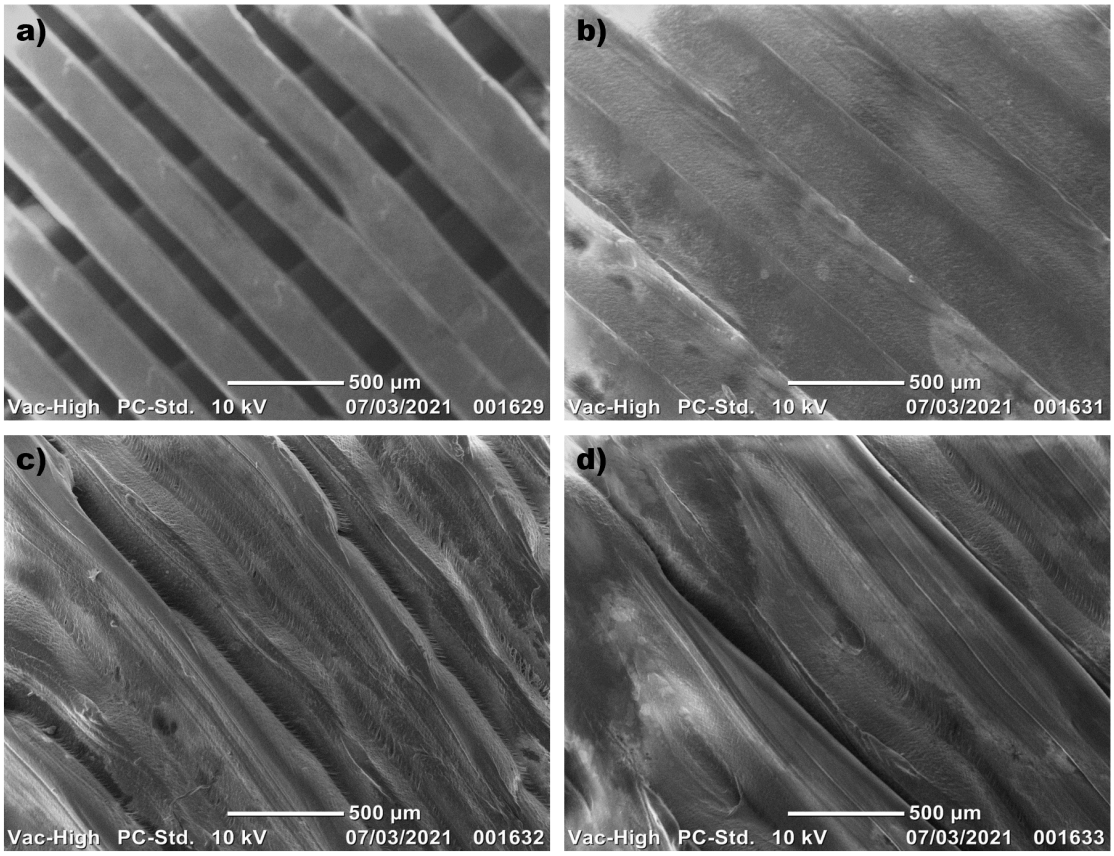

Figure 14: SEM micrographs for PLA specimens printed at 200°C: a) 70% flow; b) 100% flow; c) 130% flow; d) 160% flow

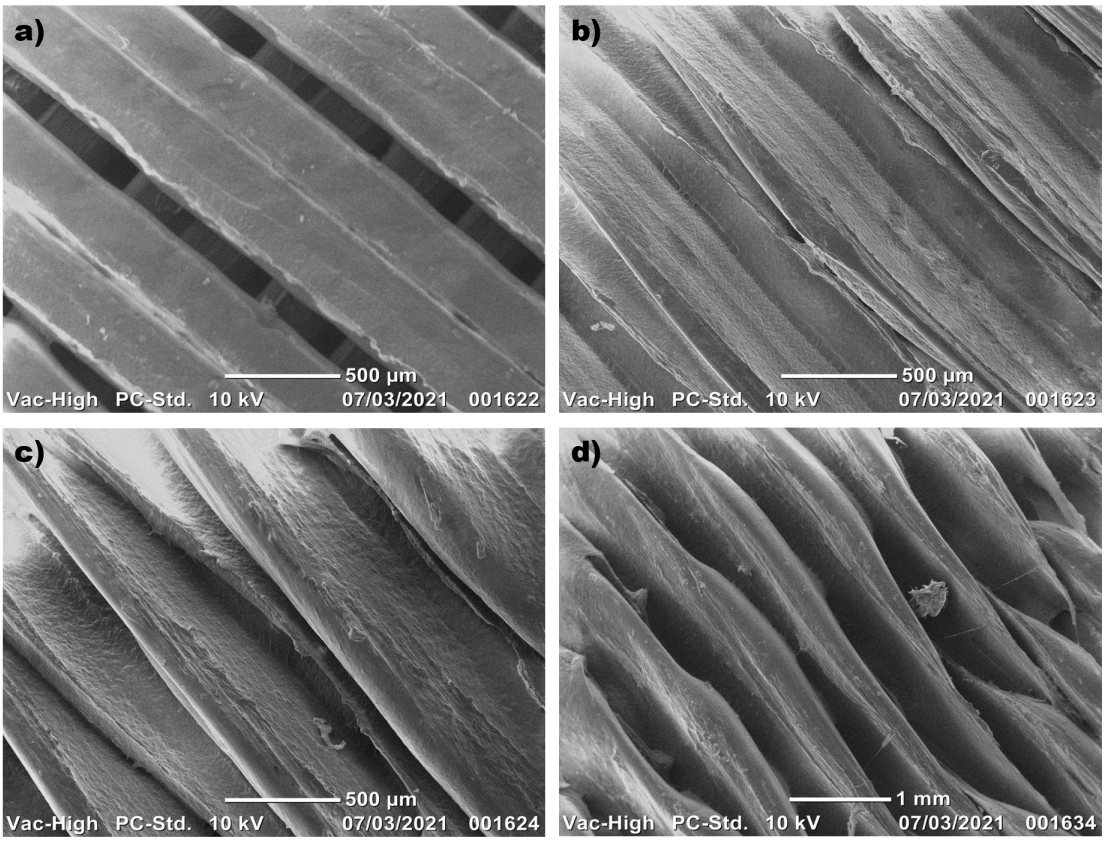

Figure 15: SEM micrographs for GPLA specimens printed at 200°C: a) 70% flow; b) 100% flow; c) 130% flow; d) 160% flow

After the surfaces had been analysed for PLA and GPLA printed at 200 °C, the fractured surfaces from the tensile test were also observed under the SEM. Figure 16 shows the SEM micrographs for the PLA material. A clean fracture surface with large voids between the layers can be observed in Fig. 16a (70% flow). The clean fracture is delamination failure indicating that the bond between the layers delaminated before the bulk strength of the material was reached. As can be seen in Fig. 16b, the 100% flow specimen failed in a completely different manner, creating a rough surface with failure occurring across many different layers. The same can be observed for specimens printed at 130% flow (Fig. 16c) and 160% flow (Fig. 16d). This rough surface indicates that the failure relates to the bulk material properties of the material. These specimens did not fail completely due to bond strength, but due to a combination of bond strength and bulk material failure [42]. The fractured surfaces of GPLA specimens printed at 200 °C are shown in Fig. 17. Upon comparison with PLA, the difference is clear for 70% flow specimens. GPLA exhibited higher fracture load values at 70% flow compared to PLA by creating a rough surface at fracture (Fig. 17a). The remaining specimens failed similar to PLA with rough surfaces as observed in Figs. 17b (100% flow), 17c (130% flow) and 17d (160% flow).

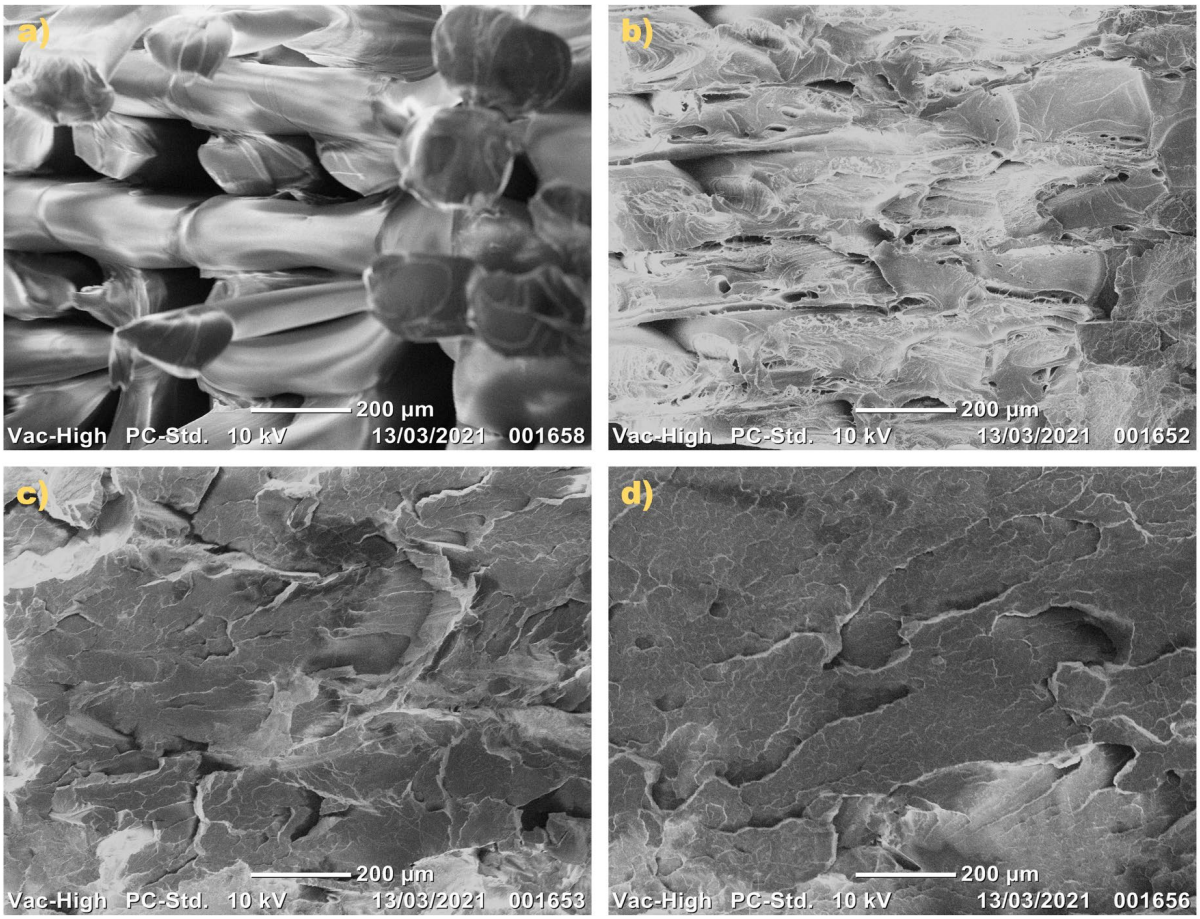

Figure 16: SEM micrographs for fractured PLA specimens printed at 200 °C: a) 70% flow; b) 100% flow; c) 130% flow; d) 160% flow

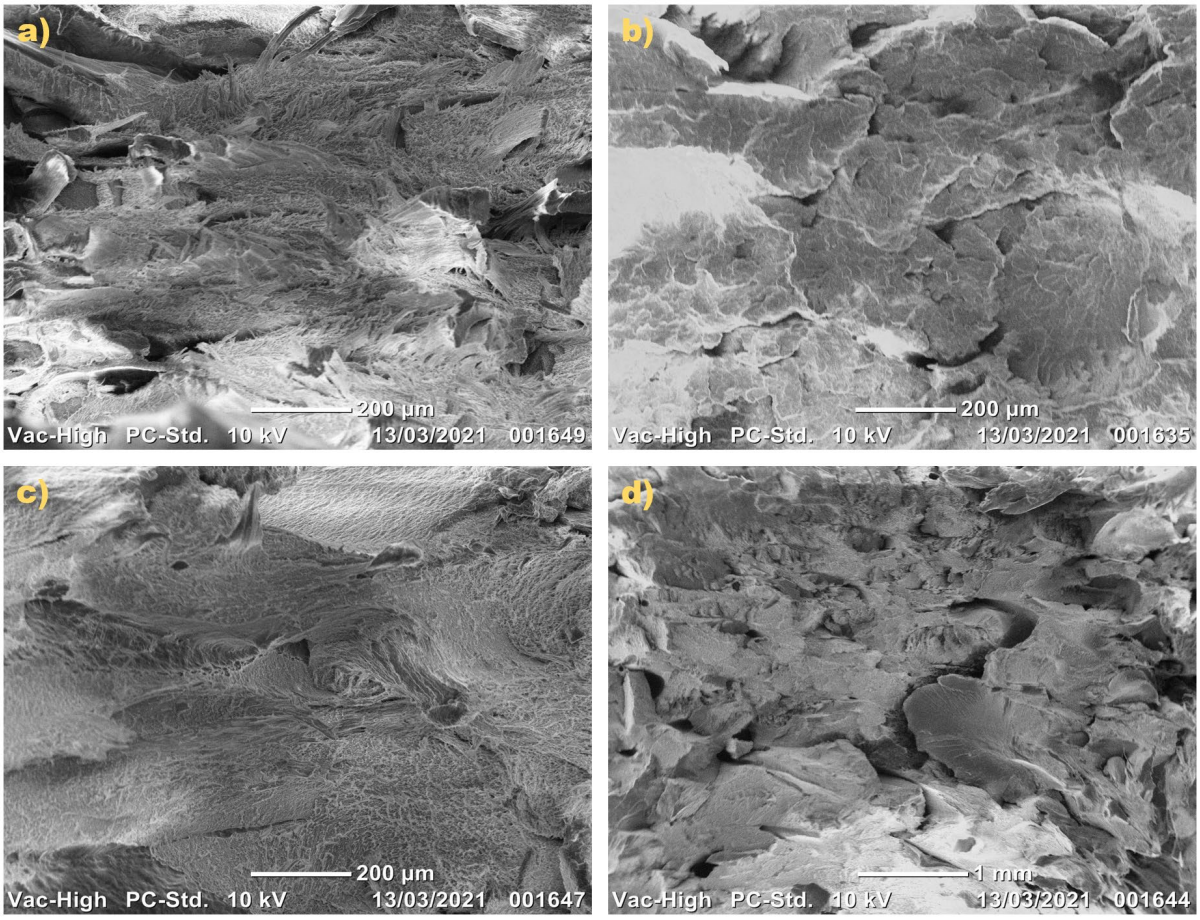

Figure 17: SEM micrographs for fractured GPLA specimens printed at 200 °C: a) 70% flow; b) 100% flow; c) 130% flow; d) 160% flow

4. Material Quality Characterization

This work is focused on analysing the effects of extrusion temperatures and flow percentages on FFF-printed PLA and GPLA specimens. It is aimed at providing an in-depth understanding of the trade-offs that can be made while manufacturing parts using the FFF process specifically in terms of dimensional accuracy, surface finish and tensile strength. These are common issues associated with FFF-printed parts [42, 43]. Increasing the flow percentage leads to increase in mass of a specific product as more material is being extruded within the same geometry resulting in dimensional inaccuracies. The most noticeable difference is along the Z-axis as described in Section 3.2. The results discussed in Sections 3.1 and 3.2 can help users decide how to manipulate the extrusion temperatures and flow percentages to achieve the desired geometry. Table 3 shows the extrusion temperatures and flow percentages for PLA and GPLA specimens with no geometrical variance. While all extrusion temperatures can provide specimens with no variance, the commonly used 100% flow does not ensure dimensional accuracy along all three axes. Therefore, it is crucial to understand the effects of flow percentage to manufacture a high quality product. For example, if X (length) and Z (thickness) axes are more critical to the product, then printing PLA at 180 °C with 110% flow will give the desired results. On the other hand, printing PLA at 210 °C with 90% flow will result in no variance along the X and Y (width) axes. These considerations are extremely important if a part is to be fitted within an assembly. Understanding the effects of under/over extrusion can help users remedy issues related to improper fitting within assemblies. It is also a good practice

to account for shrinkage with thermoplastics by slightly increasing the flow percentage. Some excess material (over-extruded) can be easily removed through post-processing operations. Therefore, Table 4 has been presented to show PLA and GPLA specimens with the lowest positive variance along the three axes. Combining Tables 3 and 4 show that printing PLA at 180 °C with 110% flow will give the optimal results (X and Z axes with no variance and Y-axis with the lowest positive variance). On the other hand, printing GPLA at 180 °C with 90% flow will result in parts having no variance along X and Y axes (close to the optimal value of 100% flow along the Z-axis).

Table 3: PLA and GPLA specimens with no variance

Axes	Temperature (°C)	Flow (%)
PLA		
X-axis	180	100, 110, 120
	200	90
	210	80, 90
Y-axis	180	90
	210	90
Z-axis	180	110
	190	110
	210	100
GPLA		
X-axis	180	80, 90
	210	70, 80, 90
Y-axis	180	80, 90
	190	70, 80, 90
	200	70
	210	70
Z-axis	180	100
	190	100
	200	100

Table 4: PLA and GPLA specimens with lowest positive variance

Axes	Temperature (°C)	Flow (%)
PLA		
X-axis	180	130, 140
	190	100
	200	100, 110, 120, 130
	210	100, 110
Y-axis	180	100, 110
	190	90
	200	90
	210	100
Z-axis	180	120
	190	120
	200	110
	210	110
GPLA		

X-axis	180	100
	190	100
	200	100
	210	100
Y-axis	180	100
	190	100, 110
	200	80, 90
	210	80, 90
Z-axis	180	110
	190	110
	200	110
	210	100

Combining the dimensional accuracy with surface roughness is an important aspect especially if a perfect fit within an assembly is needed. Surface roughness values (Ra) for PLA and GPLA are shown in Fig. 18 with both extrusion temperatures and flow percentages. The lowest surface roughness values for PLA have been obtained at 180 °C (4.461 µm), 190 °C (4.471 µm) and 210 °C (5.018 µm) with 90% flow (Section 3.3). However, one of the combinations providing the optimal dimensional accuracy is printing PLA at 180 °C with 110% flow as it will lead to zero variance along the X and Z axes and lowest positive variance along the Y-axis (Tables 3 and 4). Using this information, the user can manipulate the flow percentage to achieve the desired result based on the application as the extrusion temperature is the same. For example, printing GPLA at 180 °C with 90% flow will result in parts having zero variance along X and Y axes. However, Ra value at this combination is 19.371 µm. The user can choose to only modify the flow percentage to 80% and get 7.229 µm which is a considerable reduction in the surface roughness. This is the kind of trade-off that can help leverage the benefits of under and/or over extrusion to manufacture products with varied applications. If surface finish is the main consideration, then a suitable combination can be chosen by the user that could sacrifice dimensional accuracy in favour of a better surface finish.

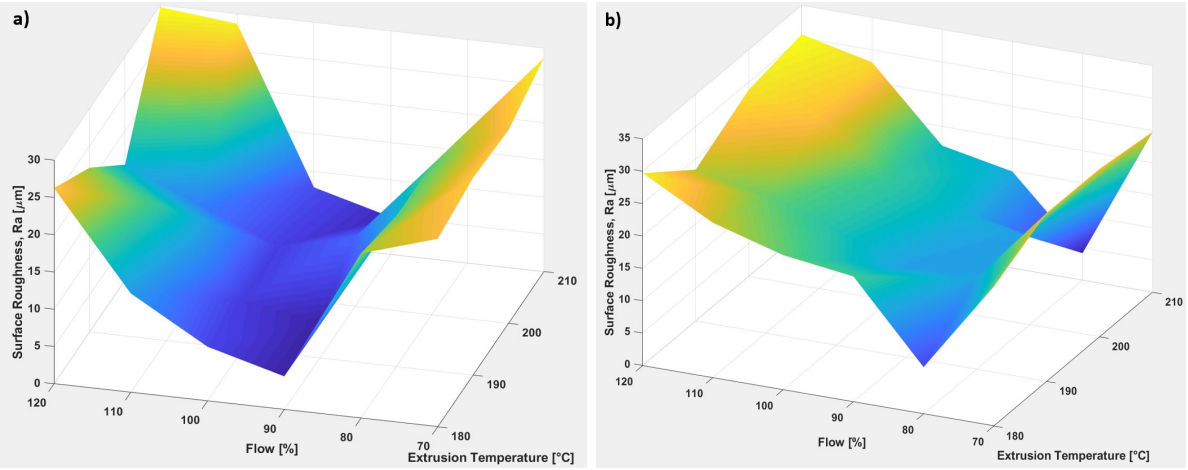

Figure 18: Surface roughness values: a) PLA material; b) GPLA material

A single attribute is comparatively easier to modify and adjust as opposed to a combination of attributes. For example, if the only consideration is surface roughness, then the results shown in Section 3.3 can help identify the extrusion temperatures and flow percentages at which parts

should be printed. Specimens with over 120% flow have extremely poor surface finish due to over-extrusion and hence should not be printed if good surface finish is the objective. As per the results, the highest surface finish has been observed at 180 °C, 190°C with 90% flow for PLA and at 210 °C with 80% flow for GPLA. These flow percentages represent under-extruded specimens, meaning a lower cross-sectional area and hence a lower load resisting capacity compared to an over-extruded specimen. Increasing the flow percentage increases the fracture load values to a limit as shown in Fig. 19. Linking this aspect with surface roughness results mean that if high tensile strength is the main goal with some focus on surface finish, then specimens printed with 120% flow are ideal for the chosen application. However, if tensile strength is the only objective with no consideration for dimensional accuracy and surface roughness, then the results in Section 3.5 clearly highlight that PLA can be printed up to 150% flow with all temperatures (except 210 °C that can provide a higher value at 160% flow) to achieve the highest tensile strength in the manufactured products.

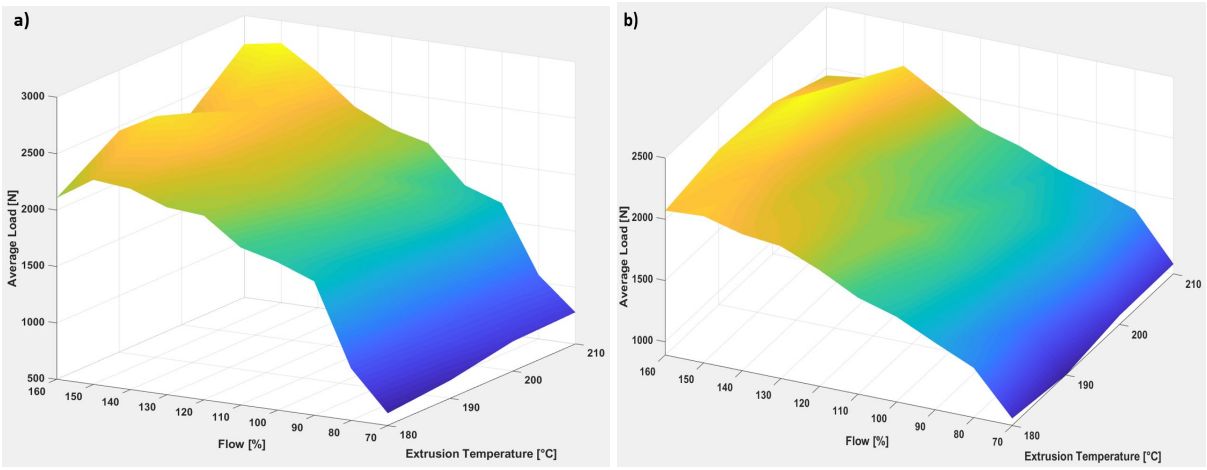

Figure 19: Tensile test results: a) PLA material; b) GPLA material

Considering a case where limits have been applied to surface roughness and fracture load values would mean that the user can plot these two parameters against each other to identify the combination of extrusion temperature and flow percentage to achieve the desired results. These plots are shown in Fig. 20 for both PLA and GPLA. The plotted points represent the combination of extrusion temperature and flow percentage with S1 indicating 180 °C at 70% flow, S2 indicating 180 °C at 80% flow, and so on until S6 that indicates 180 °C at 120% flow (maximum flow percentage due to over extrusion issues leading to poor surface finish). S7 indicates 190 °C at 70% flow and so on. Consider that a PLA product is needed with a maximum surface roughness of 12 µm and fracture load in excess of 2000N. The only combination that fulfils these requirements is 200 °C with 110% flow, indicated by S17 in Fig. 20a. The same procedure can be implemented to identify the optimal combination for GPLA products as well (Fig. 20b). These results help the user understand the limitations and identify the potential of manipulating extrusion temperature and flow percentage to achieve desired results by characterising the material quality for a specified application. They also show that the commonly used 100% flow does not always provide the optimal results and process parameters should be optimised based on the user requirements.

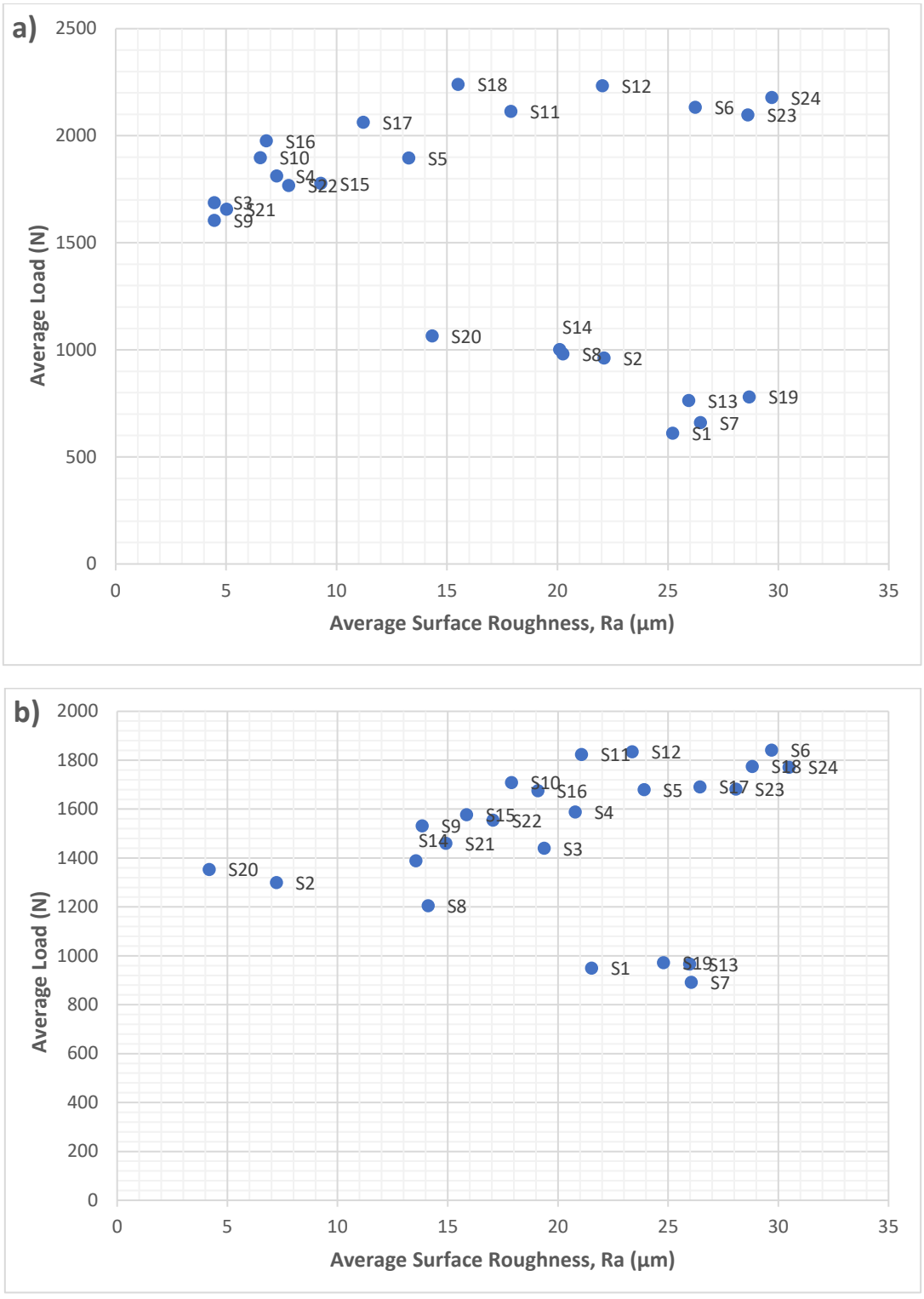

Figure 20: Average load vs average surface roughness: a) PLA material; b) GPLA material

5. Conclusions

Material extrusion rate is an important factor in FFF. However, it has not been explored to a large extent for bespoke properties. Under/over extrusion of material can lead to useful applications; thus, making the FFF process more versatile. Over extrusion, in particular, can be utilized when surface roughness or dimensional accuracy is not a consideration, and the focus

is on mechanical strength. This is because over extrusion results in tightly packed rows of extruded material leading to minimal voids and gaps between layers resulting in improved strength. Over extrusion can also be achieved by using higher extrusion temperatures. In this study, PLA and graphene enhanced PLA (GPLA) materials were investigated to analyze the effect of extrusion temperatures and material extrusion rates on their mass, dimensional accuracy, surface roughness, nondestructive defect detection and tensile properties followed by microstructural characterization. The materials were printed at four different extrusion temperatures at extrusion rates (flow percentages) ranging from 70% to 160%. The results indicate that PLA was less adversely affected due to changes in the extrusion temperatures and material extrusion rates as compared to GPLA.

The mass of GPLA specimens increased drastically with increase in flow percentages whereas PLA did not accumulate large amounts of excess material and showed lower mass values compared to the ones indicated by the Ultimaker Cura 4.7.1 software at all extrusion temperatures. With increase in mass, GPLA also experienced larger dimensional inaccuracies along the three axes (X, Y and Z) compared to PLA. All the specimens suffered from under and over extrusion that led to extremely rough surfaces. PLA material still showed lower surface roughness (Ra) values compared to GPLA. Both PLA and GPLA exhibited low surface roughness values at flow percentages lower than 100% (90% for PLA and 80% for GPLA) indicating that under extrusion is a better option to achieve the smoothest surfaces possible. Both materials showed similar mean values for surface profile ratio (Rq/Ra) whereas the standard deviation values for GPLA increased with increase in extrusion temperature.

In terms of skewness (Rsk), both PLA and GPLA followed similar trends at all extrusion temperatures by starting with negative skew for under extruded specimens, moving to an approximately symmetrical skew and finally positive skew for over extruded specimens. Similar to GPLA, PLA specimens showed leptokurtic and platykurtic distributions with the only exception that PLA specimens printed at 180 °C showed mesokurtic distribution. With regards to Rk, Rpk and Rvk characterization for PLA, 90% and 100% flow specimens exhibited the lowest values whereas 80% and 90% flow displayed the same for GPLA. Mr1 showed tiny material portion by less than 20% flat peaks whereas Mr2 showed considerable material portion by more than 80% steep valleys for PLA at all extrusion temperatures whereas GPLA showed less than 20% Mr1 for 180 °C and 210 °C and slightly over for 190 °C and 200 °C.

Ultrasonic testing highlighted the pattern of GPLA being affected more adversely compared to PLA with higher transmission times as GPLA specimens were thicker. Tensile testing for PLA yielded an increase in fracture load until 150% flow and a sharp decline moving forward. On the other hand, GPLA specimens showed different results at each extrusion temperature with no defined pattern. Microstructural analysis undertaken on the specimen surfaces and their fractured surfaces highlighted the effects of under and over extrusion. The fractured surfaces were characterized by a rough texture indicating that the failure was caused by a combination of bond strength and bulk material failure.

The results obtained in this work can help manufacturers design and develop products using different materials based on bespoke requirements. It has been demonstrated that different extrusion temperatures and material extrusion rates can lead to useful results. Three

main aspects of consideration for FFF parts are dimensional accuracy, surface finish and mechanical strength. They can be manipulated based on the product requirements, and different extrusion temperatures as well as extrusion rates can be utilized to achieve desired results.

Declarations

Author Contributions: J.B. conceptualised the idea, designed the methodology, undertook data curation, investigation, formal analysis, project administration, manuscript writing, reviewing and editing; R.B. and V.M. undertook data curation, investigation, and acquired resources.

Funding: This research did not receive any external funding.

Conflicts of Interest: The authors declare no conflict of interest.

Availability of data and material: The data has been saved in the Anglia Ruskin University's research repository.

Code availability: Not applicable.

References

1. Attar, H., Ehtemam-Haghighi, S., Soro, N., Kent, D. and Dargusch, M.S., 2020. Additive manufacturing of low-cost porous titanium-based composites for biomedical applications: Advantages, challenges and opinion for future development. *Journal of Alloys and Compounds*, *827*, p.154263. https://doi.org/10.1016/j.jallcom.2020.154263
2. Sabahi, N., Chen, W., Wang, C.H., Kruzic, J.J. and Li, X., 2020. A review on additive manufacturing of shape-memory materials for biomedical applications. *Jom*, *72*(3), pp.1229-1253. https://doi.org/10.1007/s11837-020-04013-x
3. Butt, J., 2020. Exploring the interrelationship between additive manufacturing and Industry 4.0. *Designs*, *4*(2), p.13. https://doi.org/10.3390/designs4020013
4. Ryan, K.R., Down, M.P. and Banks, C.E., 2020. Future of additive manufacturing: overview of 4D and 3D printed smart and advanced materials and their applications. *Chemical Engineering Journal*, p.126162. https://doi.org/10.1016/j.cej.2020.126162
5. Butt, J., Mebrahtu, H. and Shirvani, H., 2018. Numerical and experimental analysis of product development by composite metal foil manufacturing. *International Journal of Rapid Manufacturing*, *7*(1), pp.59-82. 10.1504/IJRAPIDM.2018.089729
6. Butt, J. and Shirvani, H., 2018. Additive, subtractive, and hybrid manufacturing processes. *Advances in Manufacturing and Processing of Materials and Structures; CRC Press: Boca Raton, FL, USA*, pp.187-218.
7. Boparai, K.S., Singh, R., Fabbrocino, F. and Fraternali, F., 2016. Thermal characterization of recycled polymer for additive manufacturing applications. *Composites Part B: Engineering*, *106*, pp.42-47. https://doi.org/10.1016/j.compositesb.2016.09.009
8. Butt, J.; Mebrahtu, H.; Shirvani, H. Metal Rapid Prototyping Technologies. In *Advances in Engineering Research*; Petrova, V.M., Ed.; Nova Science Publishers, Inc.: New York, NY, USA, 2017; Chapter 2, Volume 14, pp. 13–52.

9. Guo, N. and Leu, M.C., 2013. Additive manufacturing: technology, applications and research needs. *Frontiers of Mechanical Engineering*, *8*(3), pp.215-243. https://doi.org/10.1007/s11465-013-0248-8
10. Butt, J., Onimowo, D.A., Gohrabian, M., Sharma, T. and Shirvani, H., 2018. A desktop 3D printer with dual extruders to produce customised electronic circuitry. *Frontiers of Mechanical Engineering*, *13*(4), pp.528-534. https://doi.org/10.1007/s11465-018-0502-1
11. Gao, J., 2017, August. Production of multiple material parts using a desktop 3D printer. In *Advances in Manufacturing Technology XXXI: Proceedings of the 15th International Conference on Manufacturing Research, Incorporating the 32nd National Conference on Manufacturing Research, September 5–7, 2017, University of Greenwich, UK* (Vol. 6, p. 148). IOS Press.
12. Dana, H.R., Barbe, F., Delbreilh, L., Azzouna, M.B., Guillet, A. and Breteau, T., 2019. Polymer additive manufacturing of ABS structure: Influence of printing direction on mechanical properties. *Journal of Manufacturing Processes*, *44*, pp.288-298. https://doi.org/10.1016/j.jmapro.2019.06.015
13. Zhao, Y., Chen, Y. and Zhou, Y., 2019. Novel mechanical models of tensile strength and elastic property of FDM AM PLA materials: Experimental and theoretical analyses. *Materials & Design*, *181*, p.108089. https://doi.org/10.1016/j.matdes.2019.108089
14. Dickson, A.N., Barry, J.N., McDonnell, K.A. and Dowling, D.P., 2017. Fabrication of continuous carbon, glass and Kevlar fibre reinforced polymer composites using additive manufacturing. *Additive Manufacturing*, *16*, pp.146-152. https://doi.org/10.1016/j.addma.2017.06.004
15. Young, D., Wetmore, N. and Czabaj, M., 2018. Interlayer fracture toughness of additively manufactured unreinforced and carbon-fiber-reinforced acrylonitrile butadiene styrene. *Additive Manufacturing*, *22*, pp.508-515. https://doi.org/10.1016/j.addma.2018.02.023
16. Chacón, J.M., Caminero, M.A., García-Plaza, E. and Núnez, P.J., 2017. Additive manufacturing of PLA structures using fused deposition modelling: Effect of process parameters on mechanical properties and their optimal selection. *Materials & Design*, *124*, pp.143-157. https://doi.org/10.1016/j.matdes.2017.03.065
17. Gonabadi, H., Yadav, A. and Bull, S.J., 2020. The effect of processing parameters on the mechanical characteristics of PLA produced by a 3D FFF printer. *The International Journal of Advanced Manufacturing Technology*, *111*(3), pp.695-709. https://doi.org/10.1007/s00170-020-06138-4
18. Wu, W., Ye, W., Wu, Z., Geng, P., Wang, Y. and Zhao, J., 2017. Influence of layer thickness, raster angle, deformation temperature and recovery temperature on the shape-memory effect of 3D-printed polylactic acid samples. *Materials*, *10*(8), p.970. 10.3390/ma10080970
19. Butt, J., Hewavidana, Y., Mohaghegh, V., Sadeghi-Esfahlani, S. and Shirvani, H., 2019. Hybrid manufacturing and experimental testing of glass fiber enhanced thermoplastic composites. *Journal of Manufacturing and Materials Processing*, *3*(4), p.96. https://doi.org/10.3390/jmmp3040096

20. Heidari-Rarani, M., Rafiee-Afarani, M. and Zahedi, A.M., 2019. Mechanical characterization of FDM 3D printing of continuous carbon fiber reinforced PLA composites. *Composites Part B: Engineering*, *175*, p.107147. https://doi.org/10.1016/j.compositesb.2019.107147
21. Yu, S., Hwang, Y.H., Hwang, J.Y. and Hong, S.H., 2019. Analytical study on the 3D-printed structure and mechanical properties of basalt fiber-reinforced PLA composites using X-ray microscopy. *Composites Science and Technology*, *175*, pp.18-27. https://doi.org/10.1016/j.compscitech.2019.03.005
22. Mohan, V.B., Lau, K.T., Hui, D. and Bhattacharyya, D., 2018. Graphene-based materials and their composites: A review on production, applications and product limitations. *Composites Part B: Engineering*, *142*, pp.200-220. https://doi.org/10.1016/j.compositesb.2018.01.013
23. Caminero, M.Á., Chacón, J.M., García-Plaza, E., Núñez, P.J., Reverte, J.M. and Becar, J.P., 2019. Additive manufacturing of PLA-based composites using fused filament fabrication: Effect of graphene nanoplatelet reinforcement on mechanical properties, dimensional accuracy and texture. *Polymers*, *11*(5), p.799. https://doi.org/10.3390/polym11050799
24. Tanikella, N.G., Wittbrodt, B. and Pearce, J.M., 2017. Tensile strength of commercial polymer materials for fused filament fabrication 3D printing. *Additive Manufacturing*, *15*, pp.40-47. https://doi.org/10.1016/j.addma.2017.03.005
25. Jin, Z., Zhang, Z. and Gu, G.X., 2019. Autonomous in-situ correction of fused deposition modeling printers using computer vision and deep learning. *Manufacturing Letters*, *22*, pp.11-15. https://doi.org/10.1016/j.mfglet.2019.09.005
26. Forman, J., Dogan, M.D., Forsythe, H. and Ishii, H., 2020, October. DefeXtiles: 3D Printing Quasi-Woven Fabric via Under-Extrusion. In *Proceedings of the 33rd Annual ACM Symposium on User Interface Software and Technology* (pp. 1222-1233).
27. PrimaValue™ PLA. Available online: https://primacreator.com/collections/pla (accessed on 04 April 2021).
28. Haydale. Available online: https://www.haydale.com/products/ (accessed on 04 April 2021).
29. Ultimaker Cura: Advanced 3D Printing Software, Made Accessible. Available online: https://ultimaker.com/en/products/ultimaker-cura-software (accessed on 04 April 2021).
30. BS EN ISO 527-2:2012. *Plastics—Determination of Tensile Properties–Part 2: Test Conditions for Moulding and Extrusion Plastics*; British, European and International Standard: London, UK, 2012.
31. Mitutoyo: Surftest SJ-210 [inch/mm]. Available online: https://www.mitutoyo.com/wp-content/uploads/2016/09/J-section-Surftest.pdf (accessed on 04 April 2021).
32. ISO 4287:1997. *Geometrical Product Specifications (GPS) — Surface texture: Profile method — Terms, definitions and surface texture parameters*; British, European and International Standard: London, UK, 2015.
33. ISO 13565-2:1996. *Geometrical Product Specifications (GPS) — Surface texture: Profile method; Surfaces having stratified functional properties — Part 2: Height characterization using the linear material ratio curve;* British, European and International Standard: London, UK, 2012.

34. Dong, W.P., Sullivan, P.J. and Stout, K.J., 1992. Comprehensive study of parameters for characterizing three-dimensional surface topography I: Some inherent properties of parameter variation. *Wear*, *159*(2), pp.161-171. https://doi.org/10.1016/0043-1648(94)90128-7
35. Dong, W.P., Sullivan, P.J. and Stout, K.J., 1993. Comprehensive study of parameters for characterizing three-dimensional surface topography II: Statistical properties of parameter variation. *Wear*, *167*(1), pp.9-21. https://doi.org/10.1016/0043-1648(94)90127-9
36. Dong, W.P., Sullivan, P.J. and Stout, K.J., 1994. Comprehensive study of parameters for characterising three-dimensional surface topography: III: Parameters for characterising amplitude and some functional properties. *Wear*, *178*(1-2), pp.29-43. https://doi.org/10.1016/0043-1648(94)90127-9
37. Dong, W.P., Sullivan, P.J. and Stout, K.J., 1994. Comprehensive study of parameters for characterising three-dimensional surface topography: IV: Parameters for characterising spatial and hybrid properties. *Wear*, *178*(1-2), pp.45-60. https://doi.org/10.1016/0043-1648(94)90128-7
38. Thomas, T.R., 1981. Characterization of surface roughness. *Precision Engineering*, *3*(2), pp.97-104. https://doi.org/10.1016/0043-1648(62)90002-9
39. Test Equipment Center: Proceq PUNDIT PL-200. http://testequipmentscenter.com/index.php?route=product/product&product_id=76
40. Alsoufi, M.S. and Elsayed, A.E., 2018. Surface roughness quality and dimensional accuracy—a comprehensive analysis of 100% infill printed parts fabricated by a personal/desktop cost-effective FDM 3D printer. *Materials Sciences and Applications*, *9*(1), pp.11-40. 10.4236/msa.2018.91002
41. Alsoufi, M.S. and Elsayed, A.E., 2018. Quantitative analysis of 0% infill density surface profile of printed part fabricated by personal FDM 3D printer. *International Journal of Engineering & Technology*, *7*(1), pp.44-52. 10.14419/ijet.v7i1.8345
42. Butt, J. and Bhaskar, R., 2020. Investigating the Effects of Annealing on the Mechanical Properties of FFF-Printed Thermoplastics. *Journal of Manufacturing and Materials Processing*, *4*(2), p.38. https://doi.org/10.3390/jmmp4020038
43. García, E., Nunez, P.J., Chacon, J.M., Caminero, M.A. and Kamarthi, S., 2020. Comparative study of geometric properties of unreinforced PLA and PLA-Graphene composite materials applied to additive manufacturing using FFF technology. *Polymer Testing*, *91*, p.106860. https://doi.org/10.1016/j.polymertesting.2020.106860